Neurobiology of Disease

Ventrolateral Periaqueductal Gray Astrocytes Regulate Nociceptive Sensation and Emotional Motivation in Diabetic Neuropathic Pain

Lan Yang,[1*] Jingshan Lu,[1,2*] Jianpeng Guo,[1*] Jian Chen,[1] Fangfang Xiong,[1] Xinyao Wang,[1] Li Chen,[1,3] and Changxi Yu[1,3]

[1]Department of Pharmacology, School of Pharmacy, Fujian Medical University, Fuzhou, 350122, Fujian China, [2]Fujian Center for Safety Evaluation of New Drug, Fujian Medical University, Fuzhou, 350122, Fujian China, and [3]Fujian Key Laboratory of Drug Target Discovery and Structural and Functional Research, Fujian Medical University, Fuzhou, 350122, Fujian China

Diabetic neuropathic pain (DNP) is a diabetes complication experienced by many patients. Ventrolateral periaqueductal gray (vlPAG) neurons are essential mediators of the descending pain modulation system, yet the role of vlPAG astrocytes in DNP remains unclear. The present study applied a multidimensional approach to elucidate the role of these astrocytes in DNP. We verified the activation of astrocytes in different regions of the PAG in male DNP-model rats. We found that only astrocytes in the vlPAG exhibited increased growth. Furthermore, we described differences in vlPAG astrocyte activity at different time points during DNP progression. After the 14th day of modeling, vlPAG astrocytes exhibited obvious activation and morphologic changes. Furthermore, activation of Gq-designer receptors exclusively activated by a designer drug (Gq-DREADDs) in vlPAG astrocytes in naive male rats induced neuropathic pain-like symptoms and pain-related aversion, whereas activation of Gi-DREADDs in vlPAG astrocytes in male DNP-model rats alleviated sensations of pain and promoted pain-related preference behavior. Thus, bidirectional manipulation of vlPAG astrocytes revealed their potential to regulate pain. Surprisingly, activation of Gi-DREADDs in vlPAG astrocytes also mitigated anxiety-like behavior induced by DNP. Thus, our results provide direct support for the hypothesis that vlPAG astrocytes regulate diabetes-associated neuropathic pain and concomitant anxiety-like behavior.

Key words: **astrocytes; chemogenetic; diabetic neuropathic pain; emotional motivation; ventrolateral periaqueductal gray**

Significance Statement

Many studies examined the association between the ventrolateral periaqueductal gray (vlPAG) and neuropathic pain. However, few studies have focused on the role of vlPAG astrocytes in diabetic neuropathic pain (DNP) and DNP-related emotional changes. This work confirmed the role of vlPAG astrocytes in DNP by applying a more direct and robust approach. We used chemogenetics to bidirectionally manipulate the activity of vlPAG astrocytes and revealed that vlPAG astrocytes regulate DNP and pain-related behavior. In addition, we discovered that activation of Gi-designer receptors exclusively activated by a designer drug in vlPAG astrocytes alleviated anxiety-like behavior induced by DNP. Together, these findings provide new insights into DNP and concomitant anxiety-like behavior and supply new therapeutic targets for treating DNP.

Received May 17, 2022; revised Sep. 6, 2022; accepted Sep. 11, 2022.

Author contributions: L.Y., L.C., and C.Y. designed research; L.Y., J.L., J.G., J.C., F.X., and X.W. performed research; L.Y., J.L., and J.G. analyzed data; L.Y. wrote the first draft of the paper; L.Y., J.L., L.C., and C.Y. edited the paper; L.Y. wrote the paper.

This study is supported by National Natural Science Foundation of China, Grant/Award Numbers: 81973309 and 81701307; The Joint Funds for the Innovation of Science and Technology, Fujian Province, Grant/Award Numbers: 2020Y9010; Fujian Medical University Startup Fund for Scientific Research, Grant/Award Numbers: 2020QH1257.

*L.Y., J.L., and J.G. contributed equally to this work as co-first authors.

The authors declare no competing financial interests.

Correspondence should be addressed to Changxi Yu at changxiyu@mail.fjmu.edu.cn or Li Chen at lichen@fjmu.edu.cn.

https://doi.org/10.1523/JNEUROSCI.0920-22.2022

Introduction

Neuropathic pain (NP) has recently been defined as "pain caused by a lesion or disease of the somatosensory nervous system" (IASP, 2022); it is an unpleasant, continuous physiological and psychological sensation. NP frequently manifests as spontaneous pain, allodynia, and hyperalgesia (Jensen and Finnerup, 2014; Finnerup et al., 2021). A variety of conditions lead to NP, including trigeminal neuralgia, postherpetic neuralgia, chemotherapy, and diabetes (Colloca et al., 2017). Among these conditions, diabetic-induced neuropathy appears the most intractable. Diabetic peripheral neuropathy (DPN) is a common clinical complication that afflicts nearly half of individuals with diabetes (Pop-Busui et

al., 2017; Selvarajah et al., 2019). Limited data suggest that the prevalence of DPN ranges from 15.98% to 34.86% in China (F. Liu et al., 2010; Li et al., 2015; Pan et al., 2018; Y. Lu et al., 2020). The prevalence of DPN in European individuals seems to be higher (J. Sun et al., 2020). The widespread neurologic complications of diabetes necessitate the development of curative treatments and elucidation of the pathogenic mechanism.

Distally symmetric polyneuropathy may be the most common subclass of DPN (Tesfaye et al., 2013; Feldman et al., 2019) and is characterized by symmetric and distance-dependent symptoms (Dyck et al., 2011). Diabetic NP (DNP) is one of the most aversive clinical symptoms of distally symmetric polyneuropathy and may be the first symptom for which most diabetes patients seek medical help (Abbott et al., 2011; Pop-Busui et al., 2017). A multicenter cross-sectional study showed that 73.11% of diabetic patients in China developed moderate to severe DNP (Y. Zhang et al., 2021). Typical DNP symptoms include feelings of tingling, burning, and electric shock (Feldman et al., 2019). Additionally, comorbidities, such as sleep disturbances, anxiety, and depression, often accompany these painful symptoms (Colloca et al., 2017). Therefore, effective treatment of DNP and DNP-related emotional comorbidities may significantly improve patients' quality of life.

The periaqueductal gray (PAG) is an important node of the descending pain modulation pathway. Because of its location in the brain, the PAG plays a role in linking upstream and downstream regions (Morgan et al., 2008; Cheriyan and Sheets, 2018). Some studies have reported that the ventrolateral PAG (vlPAG) is a critical subnucleus for NP (Samineni et al., 2017; J. Huang et al., 2019; Y. Sun et al., 2020; J. B. Yin et al., 2020; Yu et al., 2021). Thus, the vlPAG may play a regulatory role in DNP.

Most studies on NP have focused on changes in neurons. However, the involvement of astrocytes, the most abundant glial cell type in the CNS, has received less attention (Herculano-Houzel, 2014). Because of the vast number of astrocytes in the CNS and their extensive connectivity with other neuronal cells and blood vessels, astrocytes are able to maintain the environmental homeostasis of the CNS, providing metabolic, structural, and nutritional support (Iadecola and Nedergaard, 2007; Allen and Eroglu, 2017; Stogsdill et al., 2017; Ji et al., 2019; Bayraktar et al., 2020). However, the role of astrocytes in the occurrence and development of DNP remains unclear, as does the mechanism by which vlPAG astrocytes affect the pathologic process of DNP.

Previous studies have shown that NP is induced by various disease models (Dubový et al., 2018; Ni et al., 2019b; Micheli et al., 2021) and can lead to the activation of PAG astrocytes. A recent study showed that, in DNP-model rats, astrocytes in the vlPAG were activated (X. Liu et al., 2022). Nevertheless, most of the above studies used passive observational or drug intervention methods to estimate astrocyte function. Data supporting the direct regulation of vlPAG astrocytes are lacking. Here, we adopted chemogenetics to implement precise and specific regulation of target cells. Mechanical allodynia was measured, and morphologic analysis was used to evaluate the relationship between vlPAG astrocytes and DNP. Furthermore, pain-related anxiety and aversion were also estimated. Our results suggest that vlPAG astrocytes are an essential component of DNP development and maintenance. In addition, DNP-related anxiety and emotional motivation were regulated by vlPAG astrocytes.

Materials and Methods

Animals. Adult male Sprague–Dawley rats that weighed 180-200 g were obtained from the Laboratory Animal Center of Fujian Medical University (license no. SCXK (Min) 2016-0002, Fujian, China). The animals were kept in a room with a 12:12 light/dark cycle at 25 ± 2°C and supplied with sufficient feed and purified water. All experiments were approved by the Ethics Committee of Fujian Medical University, and were conducted in accordance with the *Guide for the care and use of laboratory animals* (National Research Council, 2010).

Reagents. Chemogenetics was conducted through a designer receptor exclusively activated by a designer drug (DREADD) system mounted on adeno-associated virus (AAV), which was used to regulate cell activity (Roth, 2016). AAV2/8-gfaABC1D-hM3D (Gq)-EGFP-WPRE-pA (2.71E + 13 vg/ml) (S0482-8-H50), AAV2/8-gfaABC1D-hM4D(Gi)-EGFP-WPRE-pA (2.47E + 13 vg/ml) (S0489-8-H50), and AAV2/8-gfaABC1D-EGFP-WPRE-pA (1.65E + 13 vg/ml) (S0246-8-H50) were obtained from Taitool Bioscience. Clozapine N-oxide (CNO, A3317) has an affinity for modified human muscarinic acetylcholine receptors (hM3D(Gq) or hM4D(Gi)) and was purchased from BrainVTA.

DNP model. The DNP model was induced by T1DM according to previously protocols from our laboratory (J. Lu et al., 2021). The T1DM model was induced by a single dose of 70 mg/kg streptozotocin (STZ, S0130, Sigma-Aldrich) injected intraperitoneally into rats fasted for 12 h. Blood glucose levels were detected 72 h after the STZ injection. Rats with blood glucose levels >16.7 mM were classified as T1DM model animals; animals with blood glucose levels <16.7 mM were excluded from the experiment. DNP was evaluated by the von Frey test as described below. Individuals whose paw withdrawal threshold (PWT) was >0.8 on the 21st day after the STZ injection compared with the blank value were excluded from the experiment. All other rats were considered DNP-model animals.

Stereotaxic surgery and virus injection. Rats were anesthetized with isoflurane (R510-22, RWD Life Science) and fixed on a stereotaxic frame (68001, RWD Life Science). A small hole was drilled in the target surgical field after the skull was exposed. Five hundred nanoliters of the virus (with a titer of 3∼5E + 12 vg/ml) was injected into the bilateral vlPAG (AP = −6.8, ML = 0.6, DV = 6.4, angle = 10°) at a rate of 62.5 nl/min using an automatic microinjector (68606, RWD Life Science). After injection, the microinjector was kept in place for an additional 8 min to allow adequate diffusion and prevent fluid overflow. Finally, the microinjector was slowly withdrawn, and the scalp was sutured. Virus expression takes ∼3 weeks; therefore, the experiment was conducted only after the DREADDs were fully expressed.

von Frey test. The PWT of rats was measured by the von Frey test following a previously reported method (Mitrirattanakul et al., 2006; J. Lu et al., 2021). Rats were placed in an elevated Plexiglas container with a grid mesh floor and acclimated for at least 30 min. The von Frey test was conducted using an electronic von Frey apparatus (2391, IITC Life Science). After the animals adapted to the environment, a von Frey filament with a 50 g upper-pressure limit was used to measure the mechanical withdrawal threshold of the rats by pressing against the middle plantar area of the right hind paw. The value shown on the screen was recorded when rats withdrew, licked their hind paw, or ran away. We recorded five readings for each rat and dropped the maximum and minimum values. The interval between each measurement was at least 5 min to prevent interference with previous measurements.

Hargreaves test. Paw withdrawal latency (PWL) was measured by the Hargreaves test (Hargreaves et al., 1988). Rats were placed in an elevated Plexiglas container with a transparent glass floor and acclimated for at least 30 min. A thermal radiation beam generated by a movable infrared source (37370-001, Ugo Basile) was focused on the middle plantar area of the hind paw. Withdrawing or licking the hind paw or running away were regarded as termination actions. The latency from the beginning of irradiation to the appearance of termination action was recorded. The radiation intensity was set so that the latency of the control animals was 8-12 s. The cutoff duration was set at 30 s to prevent tissue burns. Five trials were recorded per animal, and the maximum and minimum values were eliminated. The interval between each measurement was at least 5 min to prevent interference with previous measurements.

Conditioned place aversion (CPA) and conditioned place preference (CPP). The CPA and CPP tests were modified and conducted according

to Cunningham et al. (2006) and Zhou et al. (2019). Tests were implemented in an apparatus with two compartments (25 × 25 × 50 cm) that allowed free passage. One chamber had white walls and a flat acrylic floor, while the opposite side chamber had black walls and a grid acrylic floor. The experiment was divided into three phases: habituation, contextual conditioning, and final testing. For the CPA test, rats were allowed to explore the apparatus for 15 min on the first day (habituation). After habituation, two consecutive rounds of conditioning were performed. On days 2 and 4, naive rats were limited to the black chamber for 45 min, 2 h after intraperitoneal injection of CNO. On days 3 and 5, rats were restricted to the white chamber for 45 min, 2 h after intraperitoneal injection of saline. On the final test day, the compartments were reopened, and rats were allowed to freely roam between chambers for 15 min. For the CPP test, the conditioning phase was fine-tuned. On days 2 and 4, DNP-model rats were limited to the white chamber for 45 min, 2 h after intraperitoneal injection of CNO. On days 3 and 5, rats were limited to the black chamber for 45 min, 2 h after intraperitoneal injection of saline. Videos were recorded during the entire experimental process. Animal behavior was analyzed with SMART Video-tracking software (RRID:SCR_002852, version 3.0.03). The difference score was the difference in the time rats spent in the CNO-conditioned compartment after CNO treatment.

Open field test (OFT) and elevated plus maze test (EPMT). The OFT and EPMT were used to assess anxiety-like behavior. Rats were habituated in the testing room for 30 min. Next, a single animal was placed gently in the center of the open field or elevated plus maze and allowed free exploration for 5 min. Their movements were recorded. Behavior analysis was performed using SMART Video-tracking software. The time spent, distance traveled, and number of entries to the center of the open field and open arm of the maze were recorded.

Immunohistochemistry. The animals were killed and perfused with saline, followed by 4% PFA. Those in the virus group and control virus group were treated with CNO 4 h before death. The brain was removed and postfixed in 4% PFA for 24 h at 4°C. The fixed brain was then cryoprotected in 20% and 30% gradient sucrose at 4°C until the tissue sank in the solution. Then, the brain was embedded in optimal cutting temperature (OCT) compound (4583, Sakura Finetek) and quickly frozen with liquid nitrogen. Sections with a thickness of 30 μm were sliced on a cryostat (Leica CM1950 Cryostat, RRID:SCR_018061). The sections were blocked with 5% BSA for 30 min at room temperature. For neuronal nuclear (NeuN) and ionized calcium binding adaptor molecule 1 (Iba1), 0.3% Triton X-100 was additionally used to permeabilize the cell membrane for 20 min at room temperature. Then, the sections were incubated with anti-GFAP (1:500, Cell Signaling Technology catalog #3670, RRID:AB_561049), anti-Iba1 (1:1000, Fujifilm Wako Shibayagi catalog #019-19741, RRID:AB_839504), and anti-NeuN (1:200, Proteintech catalog #26975-1-AP, RRID:AB_2880708) antibodies at 4°C overnight. After that, CoraLite594-conjugated donkey anti-mouse (1:500, Proteintech catalog #SA00013-3, RRID:AB_2797133) and CoraLite594-conjugated donkey anti-rabbit (1:500, Proteintech catalog #SA00013-8, RRID:AB_2857367) secondary antibodies were applied to integrate with primary antibodies. Images were photographed by an inverted fluorescence microscope (DMi8, Leica Microsystems CMS) with Leica Application Suite X (RRID:SCR_013673, version 3.7.2.22 383). Three images per animal were chosen for cell counting. Three individual cells in each image were randomly selected for morphology analysis and Sholl analysis. Mean observations of each animal were recorded. Cell counts, morphology analysis, and Sholl analysis were conducted with Fiji (Schindelin et al., 2012).

Sholl analysis. Sholl analysis was performed in accordance with previous reports (Ferreira et al., 2014). The color depth of the raw images chosen was transformed to 8 bits. The threshold was adjusted, and background noise was eliminated. Then, the image was binarized, and the cytoskeleton was depicted. We took the center of the cell body as the origin and drew a series of concentric circles with steps of 1 μm. The number of intersections between each concentric circle and the cytoskeleton was recorded.

Statistics. Data were analyzed by R (R Core Team, 2021) and RStudio (RStudio Team, 2020). All statistical analyses were conducted with the rstatix (Kassambara, 2021) package in R. Two-way repeated-measures ANOVAs were used to estimate differences in blood glucose levels, weight, and PWT among groups. When there was an interaction between intragroup factors and intergroup factors, the effect of a single time point was analyzed using simple effect tests. Cell quantities, morphology, OFT and EPMT data were analyzed using one-way ANOVAs followed by Tukey's multiple comparisons tests. When the data distribution did not conform to normality, Kruskal–Wallis tests were performed instead and followed by Dunn's test for multiple comparisons. When the homogeneity of variance was unequal, Welch's ANOVA followed by Games–Howell multiple comparisons was applied. Two-way repeated-measures ANOVAs were performed to inspect group differences in the Sholl analysis. Student's unpaired *t* tests were used to analyze the CPP and CPA difference scores and the number of astrocytes in PAG subregions. Student's paired *t* tests were used to analyze the difference in duration in each compartment of the apparatus in the CPP and CPA tests. The Mann–Whitney *U* method was used when the data did not fit a normal distribution. Figures were generated by ggplot2 (Wickham, 2016) and ggsignif (Ahlmann-Eltze and Patil, 2021).

Results

T1DM model induced DNP and activated vlPAG astrocytes in rats

To simulate NP caused by DPN, we established a T1DM rat model by intraperitoneal injection of 70 mg/kg STZ and monitored blood glucose levels, weight, and PWT on days 3, 7, 14, 21, and 28 (Fig. 1*A*). Common symptoms of diabetes, such as polyphagia, polydipsia, and polyuria, were observed. The T1DM model was confirmed by the presence of stable hyperglycemia ($F_{(2.70,\ 48.57)} = 137.57$, $^{***}p < 0.001$, two-way repeated-measures ANOVA followed by simple effect test, Fig. 1*B*) and lack of weight gain ($F_{(2.31,\ 41.61)} = 111.60$, $^{***}p < 0.001$, two-way repeated-measures ANOVA followed by simple effect test, Fig. 1*C*). Furthermore, mechanical allodynia, the classic symptom of DNP, appeared 7 d after STZ administration and continued for at least 28 d ($F_{(4,\ 72)} = 7.648$, $^{***}p < 0.001$, two-way repeated-measures ANOVA followed by simple effect test, Fig. 1*D*). Thermal hyperalgesia emerged early on, while thermal hypoalgesia occurred after the STZ injection ($F_{(4,\ 72)} = 2.829$, $^{*}p = 0.031$, two-way repeated-measures ANOVA followed by simple effect test, Fig. 1*E*). To verify that astrocytes in specific subregions of the vlPAG showed significant changes in DNP-model rats, we performed immunostaining to label astrocytes in all four subregions (dorsomedial, dorsolateral, lateral, and ventrolateral) of the PAG. The results showed that only astrocytes in the vlPAG exhibited an increase in GFAP-positive staining (Fig. 1*F*, and for vlPAG, $t_{(7.28)} = 12.8$ $^{***}p < 0.001$, unpaired *t* test, Fig. 1*G*). Therefore, we speculated that astrocytes in the vlPAG may be important in promoting the development of DNP.

Changes in vlPAG astrocyte activity during DNP progression in rats

We then observed vlPAG astrocyte activation at different periods within the span of 28 d after the STZ injection. As determined by the immunolabeling, at the initial stage of DNP, ~7 d after STZ injection, the vlPAG astrocytes showed no significant activation (Fig. 2*B*). The astrocytes began to display morphologic changes 14 d after the injection. After day 21, the vlPAG astrocytes showed substantial differences in both quantity and morphology. The number and the average cell body area of GFAP-positive cells rose abruptly ($H_{(5)} = 23.228$, $^{***}p < 0.001$, Kruskal–Wallis test followed by Dunn's test, Fig. 2*C*; $F_{(5,13.6)} = 43.5$, $^{***}p < 0.001$, Welch's ANOVA followed by Games–Howell test, Fig. 2*D*), and the number of astrocyte branches increased ($H_{(5)} = 27.7$, $^{***}p < 0.001$, Kruskal–Wallis test followed by Dunn's test, Fig. 2*E*). Interestingly, as early as day 7, the maximum branch length

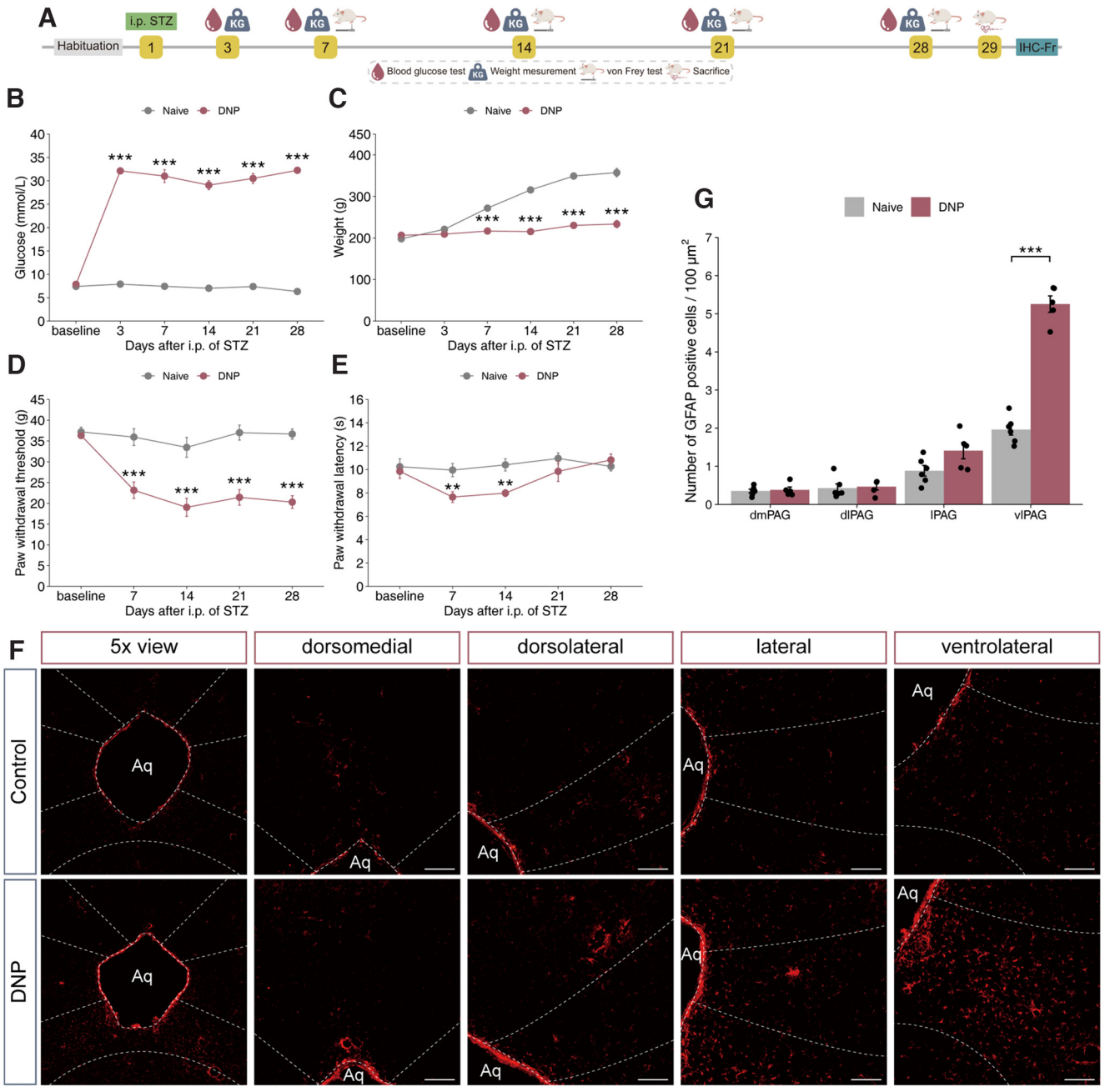

Figure 1. Activation of astrocytes in different regions of PAG in DNP rats. ***A***, Schematic of the experimental protocol. ***B***, Changes in blood glucose levels ($F_{(2.70,\ 48.57)}$ = 137.57, ***$p < 0.001$, two-way repeated-measures ANOVA followed by simple effect test, $n = 10$); ***C***, weight ($F_{(2.31,\ 41.61)}$ = 111.60, ***$p < 0.001$, two-way repeated-measures ANOVA followed by simple effect test, $n = 10$); ***D***, PWT ($F_{(4,\ 72)}$ = 7.648, ***$p < 0.001$, two-way repeated-measures ANOVA followed by simple effect test, $n = 10$); and ***E***, PWL ($F_{(4,\ 72)}$ = 2.829, *$p = 0.031$, two-way repeated-measures ANOVA followed by simple effect test, $n = 10$) in DNP-model rats after intraperitoneal injection of STZ. ***F***, Representative images of astrocyte activation in different subregions of the PAG. Scale bar, 100 μm. ***G***, Number of GFAP-positive cells in different subregions of PAG (for vlPAG $t_{(7.28)}$ = 12.8, ***$p < 0.001$, unpaired *t* test).

of astrocytes had increased ($F_{(5,30)}$ = 0.748, **$p = 0.001$, one-way ANOVA followed by Dunnett's multiple comparisons, Fig. 2*F*). Sholl analysis provided us with the cytoskeletal complexity profile that revealed that, 14 d after the STZ injection, the structural complexity of vlPAG astrocytes became progressively sophisticated ($F_{(165,\ 990)}$ = 11.827, ***$p < 0.001$, two-way repeated-measures ANOVA followed by simple effect test, Fig. 2*G*). The above results demonstrate that the activation of vlPAG astrocytes in DNP-model rats began with the extension of processes; the astrocytes then expanded in cell body size, increased in process length, and proliferated.

Activation of Gq-DREADDs in vlPAG astrocytes mimics NP-like symptoms in naive rats

However, it remains unknown whether the activation of vlPAG astrocytes triggers DNP or is a secondary result. To clarify the role of vlPAG astrocytes in pain conduction, we injected a series of AAVs carrying the DREADD sequence into the vlPAG to regulate the activation of vlPAG astrocytes (Fig. 3*A*). The majority of viruses affected local astrocytes (Fig. 3*B*,*C*), while very few virus fluorescent marker-positive cells colocalized with Iba1 and NeuN (the specific biomarker of microglia and neurons) (Fig. 3*B*,*D*,*E*). We first infected vlPAG astrocytes in naive

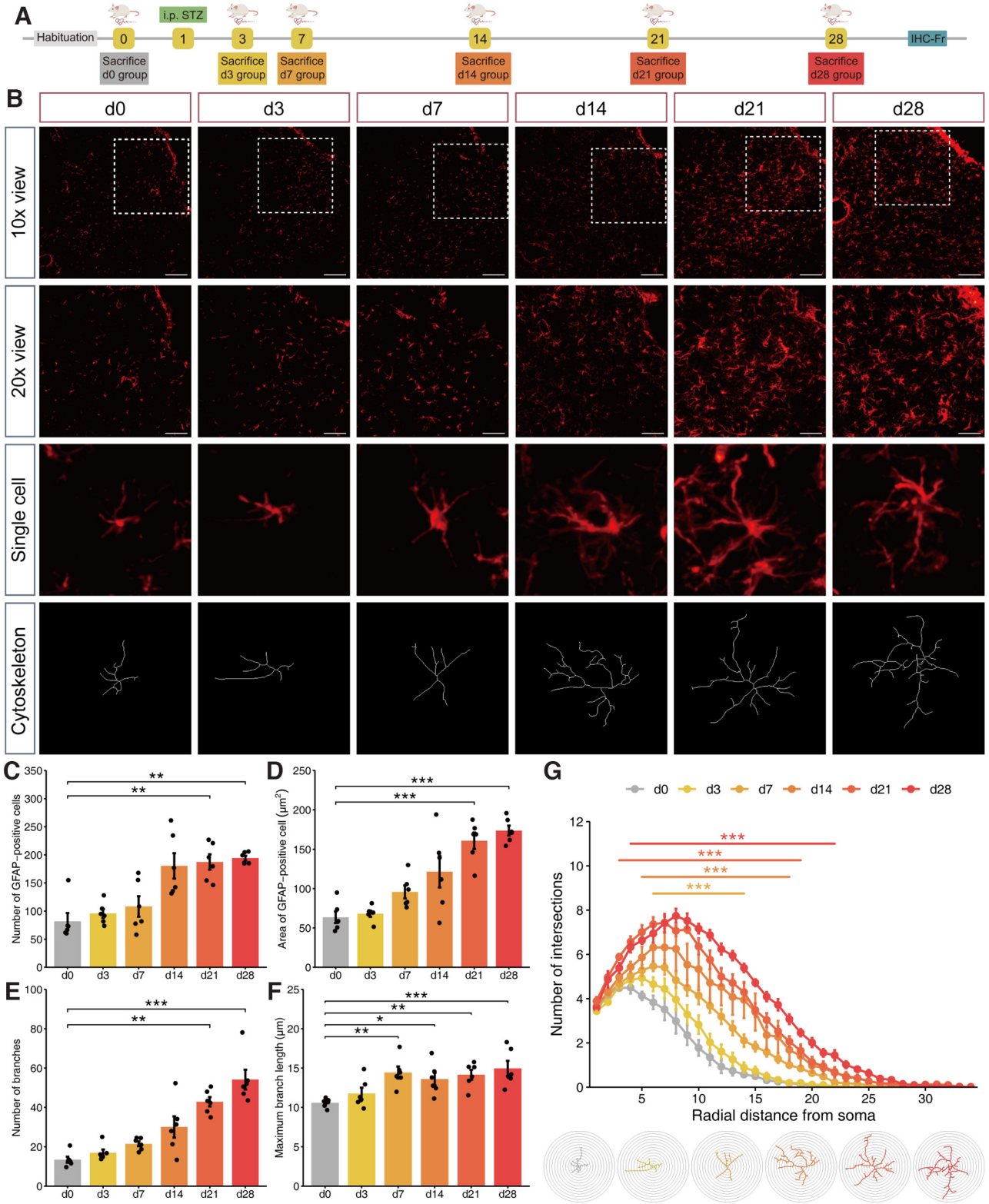

Figure 2. Characteristic of vlPAG astrocytes at different time points during DNP progression in rats. ***A***, Schematic diagram of the experimental process. ***B***, GFAP immunofluorescence staining and cytoskeleton depiction of vlPAG astrocytes at different time points after the STZ injection. Scale bars: 10× view, 100 μm; 20× view, 50 μm. ***C***, Number of GFAP-positive cells ($H_{(5)}$ = 23.228, ***$p < 0.001$, Kruskal–Wallis test followed by Dunn's test, $n = 6$). ***D***, Area of GFAP-positive cells ($F_{(5,13.6)}$ = 43.5, ***$p < 0.001$, Welch's ANOVA followed by Games–Howell test, $n = 6$). ***E***, Number of branches ($H_{(5)}$ = 27.7, ***$p < 0.001$, Kruskal–Wallis test followed by Dunn's test, $n = 6$). ***F***, Maximum branch length ($F_{(5,30)}$ = 0.748, **$p = 0.001$, one-way ANOVA followed by Dunnett's multiple comparisons, $n = 6$) of vlPAG astrocytes at different time points after the STZ injection (*$p < 0.05$, **$p < 0.01$, ***$p < 0.001$ vs day 0). ***G***, Sholl analysis of astrocytic process complexity at different time points after the STZ injection ($F_{(165, 990)}$ = 11.827, ***$p < 0.001$, two-way repeated-measures ANOVA followed by simple effect test, $n = 54$ cells in 6 rats per group, ***$p < 0.001$ vs day 0).

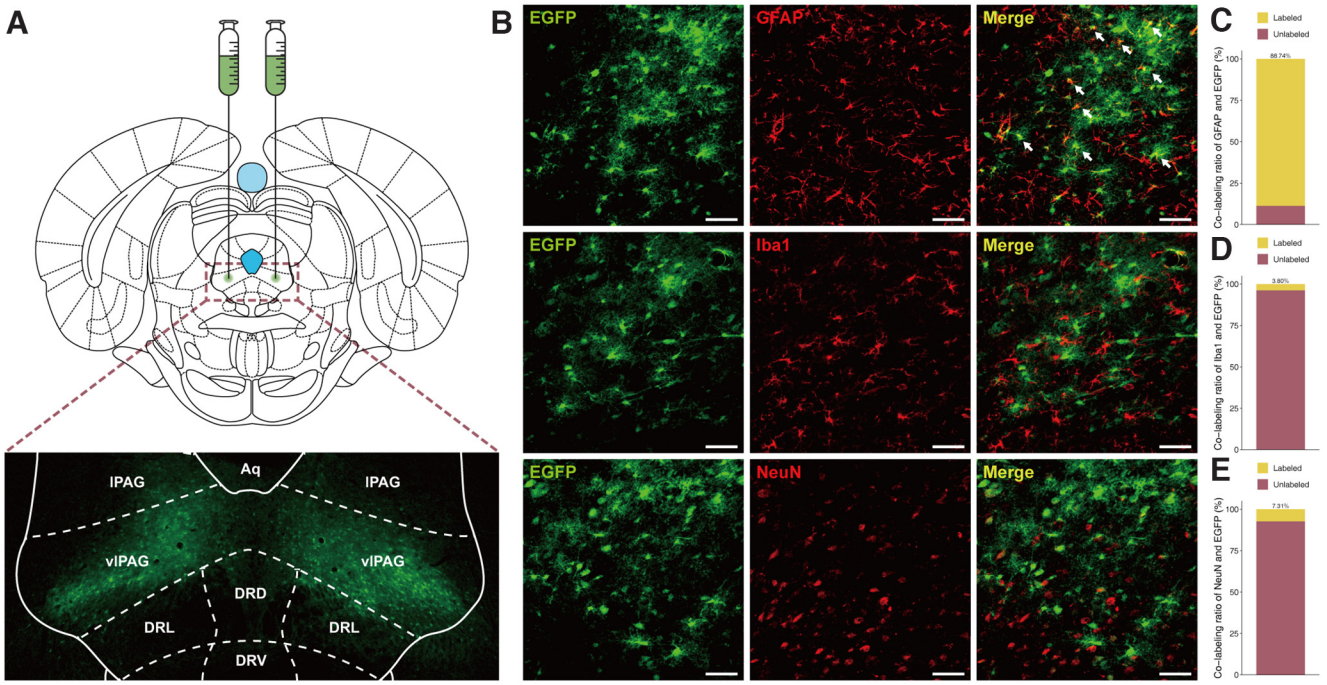

Figure 3. Verification of virus expression location and specificity. ***A***, Schematic diagram of the AAV injection site. ***B***, Representative diagram of gfaABC1D promoter-mediated expression of DREADDs and coexpression with astrocytes, microglia, and neuron-specific markers. Scale bar, 50 μm. Colabeling rate of DREADDs coupled with fluorescent signal protein: (***C***) GFAP; (***D***) Iba1; and (***E***) NeuN ($n = 6$).

rats with AAV-gfaABC1D-hM3D(Gq)-EGFP and AAV-gfaABC1D-EGFP (Fig. 4*A*,*B*). Twenty-one days after virus injection, CNO at a dose of 0.3 mg/kg was intraperitoneally injected. The PWT was determined by the von Frey test and measured once an hour for 6 consecutive hours. Following CNO administration, the PWT of the AAV-gfaABC1D-hM3D(Gq)-EGFP transfected group decreased progressively and reached a trough in the third hour. However, the PWT of the AAV-gfaABC1D-EGFP group administered CNO and the AAV-gfaABC1D-hM3D(Gq)-EGFP group administered saline showed no significant change ($F_{(30, 384)} = 5.499$ $^{***}p < 0.001$, two-way repeated-measures ANOVA followed by simple effect test, Fig. 4*C*). Immunostaining was applied to observe the characteristics of chemogenetically activated astrocytes (Fig. 4*D*). CNO administration activated astrocytes expressing hM3D(Gq), which sustained a state similar to astrocytes in the DNP model ($F_{(102, 680)} = 14.626$, $^{***}p < 0.001$ two-way repeated-measures ANOVA followed by simple effect test, Fig. 4*E*). Nonetheless, the astrocytes of the control virus group did not show significant differences from those of the naive group. We analyzed the fluorescent images and observed that the number of GFAP-positive cells rapidly increased ($F_{(3,20)} = 57.96$, $^{***}p < 0.001$, one-way ANOVA followed by Tukey's multiple comparisons, Fig. 4*F*). Additionally, the number and maximum length of astrocyte branches increased to some extent ($F_{(3,20)} = 13.273$, $^{***}p < 0.001$, one-way ANOVA followed by Tukey's multiple comparisons, Fig. 4*H*; $H_{(3)} = 17.0$, $^{**}p < 0.001$, Kruskal–Wallis test followed by Dunn's test, Fig. 4*I*). However, the average area of GFAP-positive cells in the AAV-gfaABC1D-hM3D(Gq)-EGFP group did not differ from that of the control virus group because of considerable intragroup variation ($F_{(3,9.12)} = 16.9$, $^{***}p < 0.001$, Welch's ANOVA followed by Games–Howell test, Fig. 4*G*). These results suggest that vlPAG astrocytes may be involved in NP.

Activation of Gq-DREADDs in vlPAG astrocytes induces pain-related aversion in naive rats

To confirm that activation of Gq-DREADDs in vlPAG astrocytes induced pain and pain-related emotions, we used the CPA paradigm, a relatively objective and subject-controlled experimental design to measure the aversive effect induced by hM3D(Gq) (Fig. 5*A*). CNO administration was paired with the black compartment rather than the white compartment because rodents naturally prefer dark environments. After two rounds of conditioning, the rats were allowed to freely move between the two compartments. Most rats transfected with AAV-gfaABC1D-hM3D(Gq)-EGFP spent less time in the black compartment and preferred the opposite compartment ($t_{(9)} = 4.33$, $^{**}p = 0.002$, paired t test, Fig. 5*B*,*C*), while rats in the control virus group showed no obvious preference ($t_{(9)} = 0.275$, $p = 0.789$, paired t test, Fig. 5*B*,*C*; $t_{(16.3)} = 2.30$, $^{*}p = 0.039$, unpaired t test, Fig. 5*D*). These results suggest that activation of Gq-DREADDs in vlPAG astrocytes caused NP-like symptoms and further provoked pain-related aversion.

Activation of Gi-DREADDs in vlPAG astrocytes alleviates mechanical allodynia in rats with DNP

Next, we evaluated the ability of vlPAG astrocytes to induce DNP. We injected AAV-gfaABC1D-hM4D(Gi)-EGFP and AAV-gfaABC1D-EGFP into the vlPAG immediately after STZ was intraperitoneally injected. The von Frey test was then conducted once a week to ensure that the DNP model was successfully replicated. Four weeks after the injections, CNO at a dose of 1.0 mg/kg was intraperitoneally injected. The mechanical allodynia degree was recorded by the von Frey test. As described above, the measurement was collected once an hour for 6 consecutive hours (Fig. 6*A*,*B*). After CNO administration, the PWT of DNP-model rats transfected with AAV-gfaABC1D-hM4D(Gi)-EGFP gradually increased, while that of the control virus group

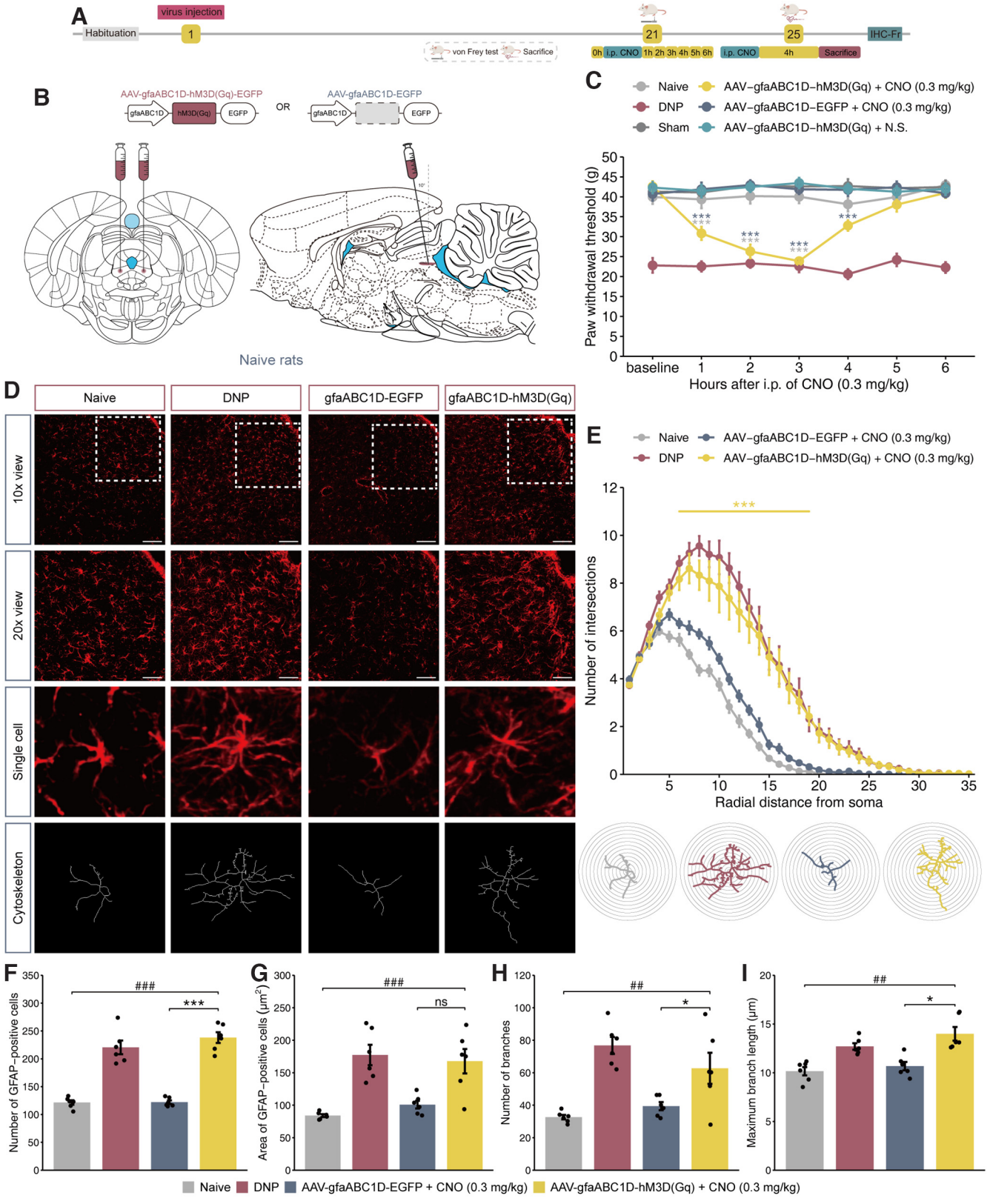

Figure 4. Gq-DREADDs selectively activate vlPAG astrocytes and induce NP-like symptoms in naive rats. ***A***, Schematic diagram of hM3D(Gq) DREADD intervention and the behavioral test process in naive rats. ***B***, Schematic diagram of the virus injection site. ***C***, The PWT trajectory during six measurements conducted at 1 h intervals in naive rats expressing gfaABC1D-hM3D(Gq)-EGFP or gfaABC1D-EGFP after intraperitoneal injection of CNO ($F_{(30, 384)} = 5.499$, $^{***}p < 0.001$, two-way repeated-measures ANOVA followed by simple effect test, $n = 10$-12, $^{***}p$ (dark blue) < 0.001 vs gfaABC1D-EGFP + CNO group, $^{***}p$ (light gray) < 0.001 vs naive group). ***D***, GFAP immunofluorescence staining and cytoskeleton depiction of vlPAG astrocytes expressing gfaABC1D-hM3D(Gq)-EGFP or gfaABC1D-EGFP after intraperitoneal injection of CNO. Scale bars: 10× view, 100 μm; 20× view, 50 μm. ***E***, Sholl analysis of astrocytes in the vlPAG expressing gfaABC1D-hM3D(Gq)-EGFP or gfaABC1D-EGFP after intraperitoneal injection of CNO ($F_{(102, 680)} = 14.626$, $^{***}p < 0.001$ two-way repeated-measures ANOVA followed by simple effect test, $n = 54$ cells per rat, 6 rats per group, $^{***}p < 0.001$ vs gfaABC1D-EGFP). ***F***, Number of GFAP-positive cells ($F_{(3,20)} = 57.96$, $^{***}p < 0.001$, one-way ANOVA followed by Tukey's multiple

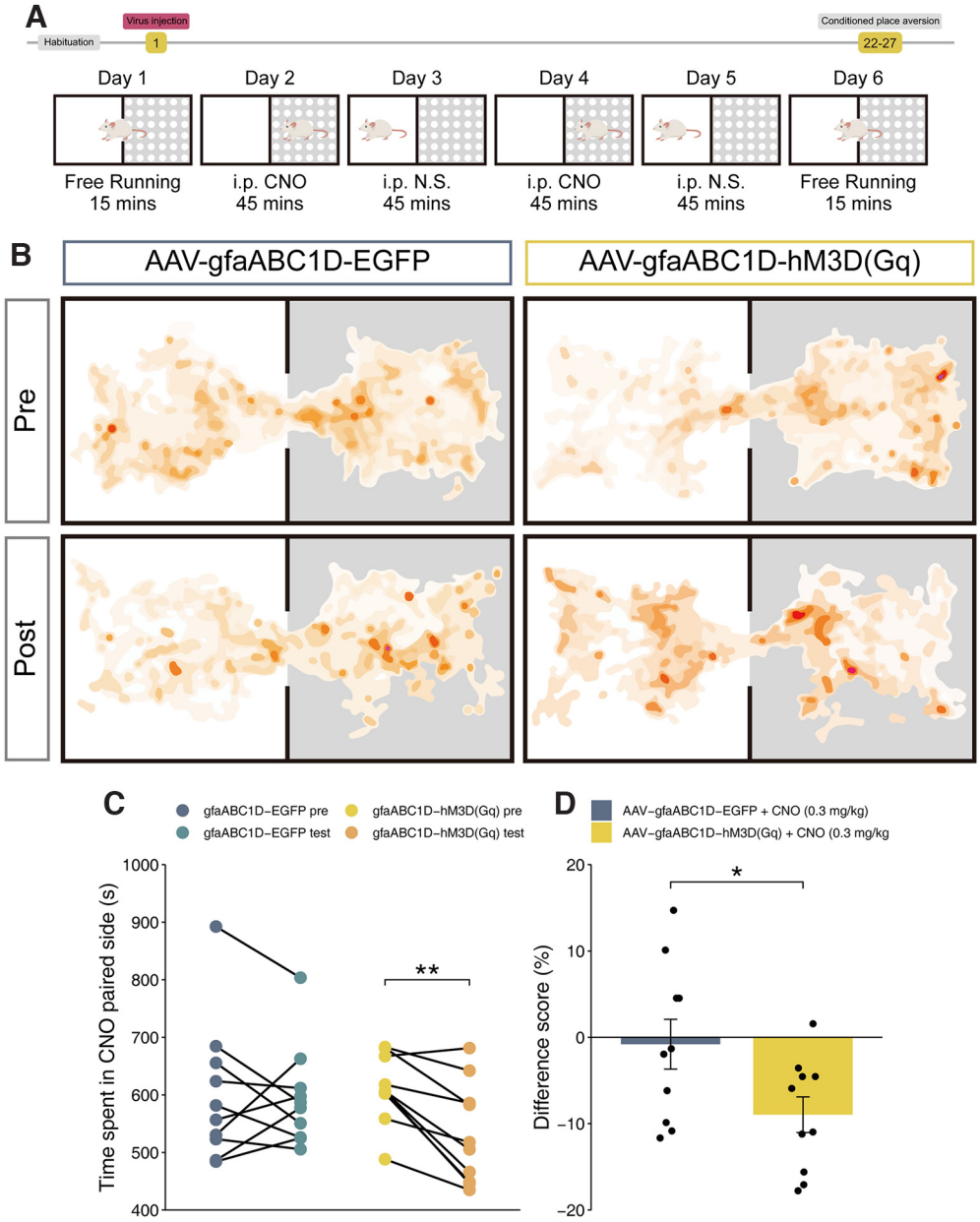

Figure 5. Gq-DREADDs selectively activate vlPAG astrocytes and induce CPA in naive rats. ***A***, Schematic diagram of the CPA testing process in naive rats. ***B***, Representative heatmap tracking the movements of naive rats expressing gfaABC1D-hM3D(Gq)-EGFP or gfaABC1D-EGFP after treatment with CNO and conditioning in the black chamber. ***C***, Time spent in the CNO-paired side (gfaABC1D-hM3D(Gq)-EGFP pretest vs test, $t_{(9)} = 4.33$, $^{**}p = 0.002$, paired *t* test, $n = 10$; gfaABC1D-EGFP pretest vs test, $t_{(9)} = 0.275$, $p = 0.789$, paired *t* test, $n = 10$). ***D***, The difference score of the CPA results ($t_{(16.3)} = 2.30$, $^{*}p = 0.039$, unpaired *t* test, $n = 10$).

maintained its initial state. The effect peaked at the third hour and lasted for 4 h ($F_{(24.81, 272.92)} = 3.027$, $^{***}p < 0.001$, two-way repeated-measures ANOVA followed by simple effect test, Fig. 6*C*). Immunofluorescence images of GFAP-positive cells were taken to ascertain the inhibitory effect of hM4D(Gi) (Fig. 6*D*). CNO administration inhibited astrocytes expressing hM4D(Gi), which showed a simpler structure than the control virus group ($F_{(102, 714)} = 9.959$, $^{***}p < 0.001$, two-way repeated-measures ANOVA followed by simple effect test, $n = 54$-63 cells in 6 or 7 rats per group, Fig. 6*E*). The number and average area of GFAP-positive cells were clearly reduced ($F_{(3,21)} = 15.151$, $^{***}p < 0.001$, one-way ANOVA followed by Tukey's multiple comparisons, Fig. 6*F*; $F_{(3,21)} = 24.759$, $^{***}p < 0.001$, one-way ANOVA followed by Tukey's multiple comparisons, Fig. 6*G*). The number of branches also decreased significantly ($F_{(3,21)} = 24.725$, $^{***}p < 0.001$, one-way ANOVA followed by Tukey's multiple comparisons, Fig. 6*H*), but no substantial differences were found in the maximum branch length ($F_{(3,21)} = 4.901$, $^{*}p = 0.01$, one-way ANOVA followed by Tukey's multiple comparisons, Fig. 6*I*). These data indicate that vlPAG astrocytes may be the fundamental factor regulating DNP. Additionally, the data suggest that the

←

comparisons, $n = 6$). ***G***, Area of GFAP-positive cells ($F_{(3,9.12)} = 16.9$, $^{***}p < 0.001$, Welch's ANOVA followed by Games–Howell test, $n = 6$). ***H***, Number of branches ($F_{(3,20)} = 13.273$, $^{***}p < 0.001$, one-way ANOVA followed by Tukey's multiple comparisons, $n = 6$). ***I***, Maximum branch length ($H_{(3)} = 17.0$, $^{**}p < 0.001$, Kruskal–Wallis test followed by Dunn's test, $n = 6$) of vlPAG astrocytes expressing gfaABC1D-hM3D(Gq)-EGFP or gfaABC1D-EGFP after intraperitoneal injection of CNO ($^{*}p < 0.05$, $^{***}p < 0.001$ vs gfaABC1D-EGFP group; $^{\#\#}p < 0.01$, $^{\#\#\#}p < 0.001$ vs naive group).

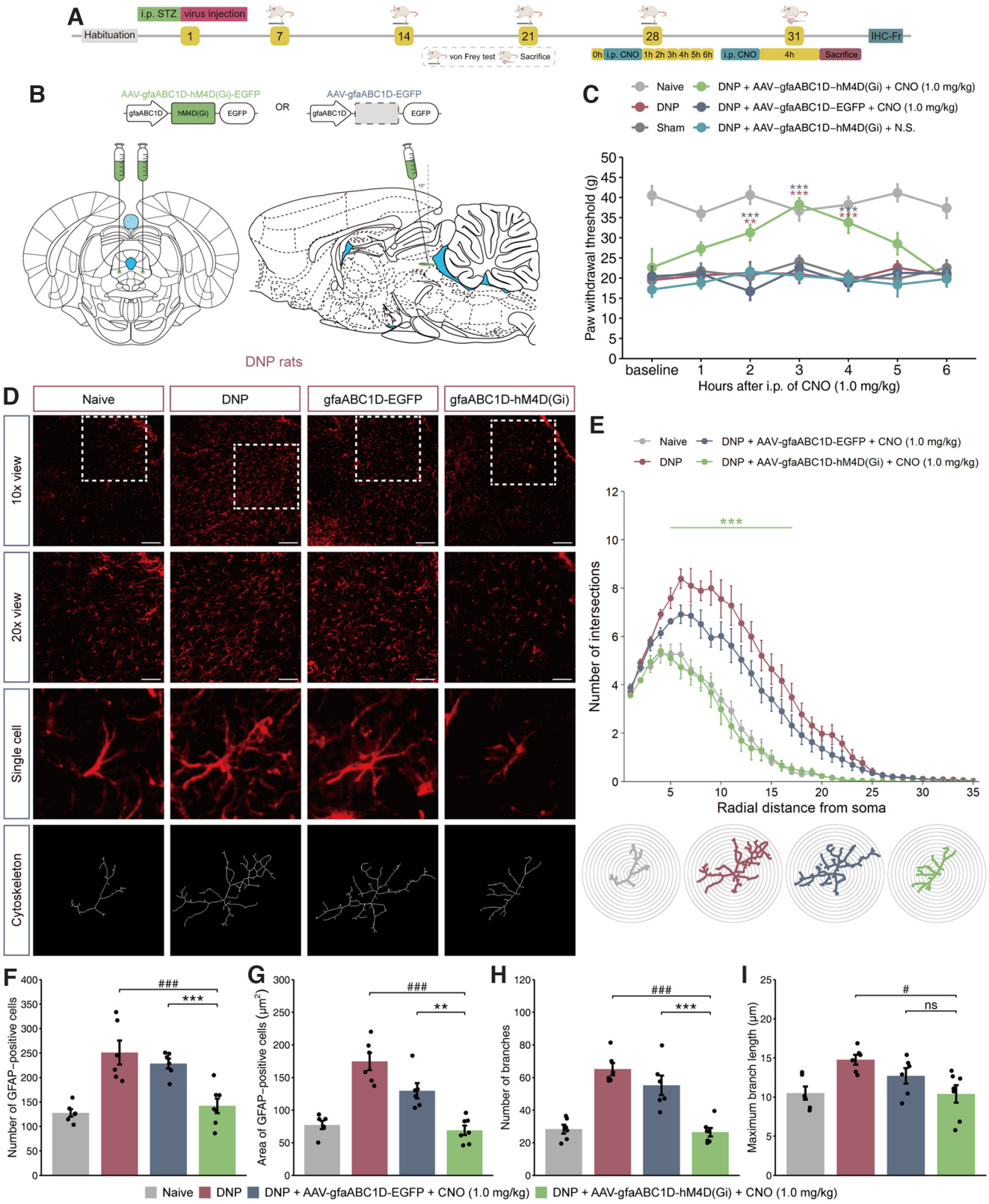

Figure 6. Gi-DREADDs selectively inhibit vlPAG astrocytes and alleviate mechanical allodynia in rats with DNP. ***A***, Schematic diagram of hM4D(Gi) DREADD intervention and the behavioral test process in naive rats. ***B***, Schematic diagram of the virus injection site. ***C***, The changes in PWT over 6 consecutive hours in DNP-model rats expressing gfaABC1D-hM4D(Gi)-EGFP or gfaABC1D-EGFP after intraperitoneal injection of CNO ($F_{(24.81, 272.92)} = 3.027$, $^{***}p < 0.001$, two-way repeated-measures ANOVA followed by simple effect test, $n = 10$, $^{***}p$ (dark blue) < 0.001 vs gfaABC1D-EGFP, $^{***}p$ (red) < 0.001 vs DNP). ***D***, GFAP immunofluorescence staining and cytoskeleton depiction of vlPAG astrocytes expressing gfaABC1D-hM4D(Gi)-EGFP or gfaABC1D-hM4D(Gi)-EGFP after intraperitoneal injection of CNO. Scale bars: 10× view, 100 μm; 20× view, 50 μm. ***E***, Sholl analysis of astrocytes in the vlPAG expressing gfaABC1D-hM4D(Gi)-EGFP or gfaABC1D-EGFP after intraperitoneal injection of CNO ($F_{(102, 714)} = 9.959$, $^{***}p < 0.001$, two-way repeated-measures ANOVA followed by simple effect test, $n = 54$-63 cells in 6 or 7 rats per group, $^{***}p < 0.001$ vs gfaABC1D-EGFP). ***F***, Number of GFAP-positive cells ($F_{(3,21)} = 15.151$, $^{***}p < 0.001$, one-way ANOVA followed by Tukey's multiple comparisons, $n = 6$ or 7). ***G***, Area of GFAP-positive cells ($F_{(3,21)} = 24.759$, $^{***}p < 0.001$, one-way ANOVA followed by Tukey's multiple comparisons, $n = 6$ or 7). ***H***, Number of branches ($F_{(3,21)} = 24.725$, $^{***}p < 0.001$,

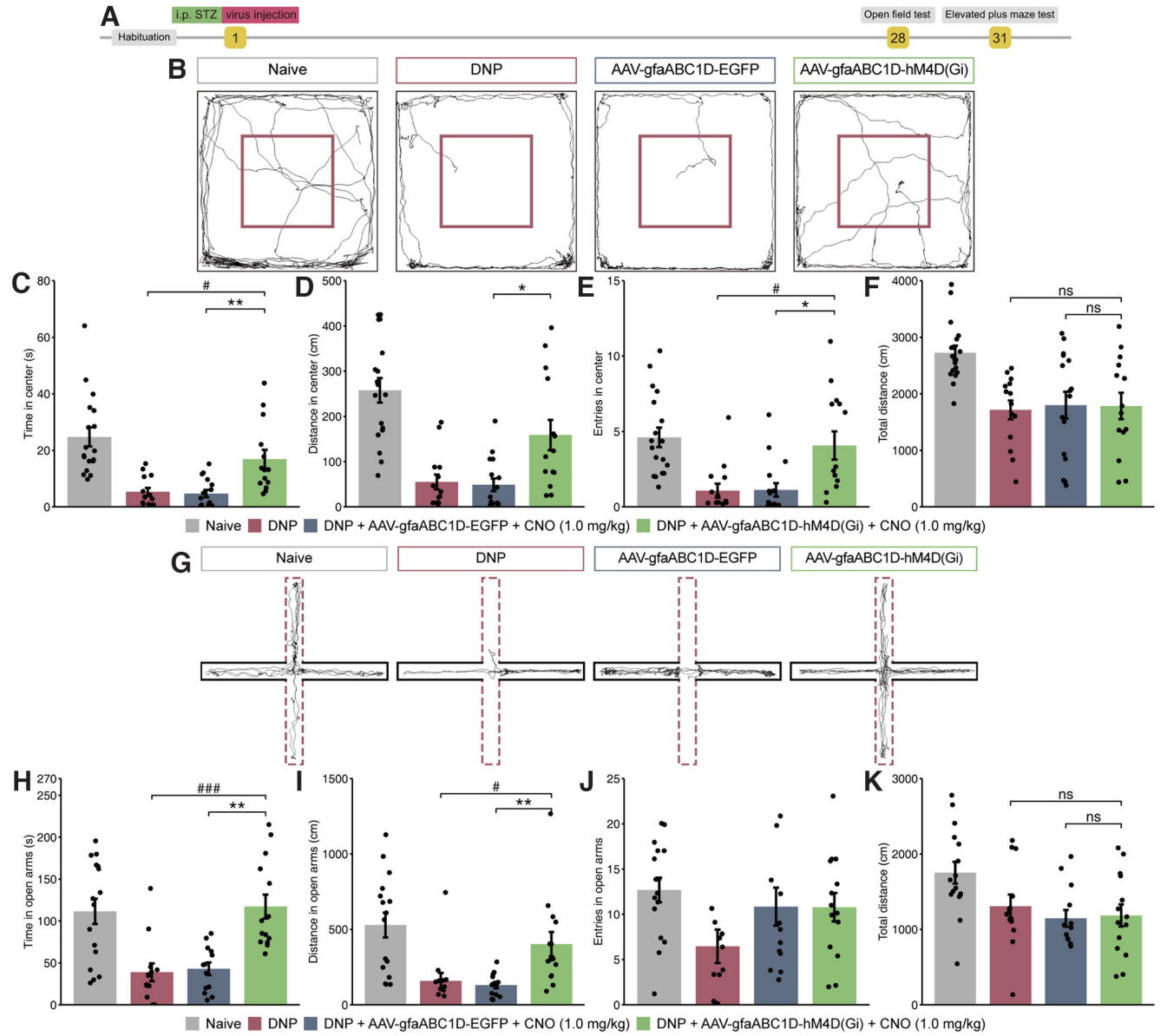

Figure 7. Inhibition of vlPAG astrocytes reverses DNP-related anxiety-like behaviors. ***A***, Schematic diagram of the OFT and EPMT used to assess DNP-model rats. ***B***, ***G***, Representative tracks of movement in DNP-model rats expressing gfaABC1D-hM4D(Gi)-EGFP or gfaABC1D-EGFP in the OFT and EPMT after administration of CNO. ***C***, Time ($H_{(3)} = 33.7$, $^{***}p < 0.001$, Kruskal–Wallis test followed by Dunn's test, $n = 14$-18). ***D***, Distance traveled ($H_{(3)} = 30.9$, $^{***}p < 0.001$, Kruskal–Wallis test followed by Dunn's test, $n = 14$-18). ***E***, Number of entries ($H_{(3)} = 23.7$, $^{***}p < 0.001$, Kruskal–Wallis test followed by Dunn's test, $n = 14$-18) in the center of the open field ($^{*}p < 0.05$, $^{**}p < 0.01$ vs gfaABC1D-EGFP group; $^{\#}p < 0.05$ vs DNP group). ***H***, Time ($H_{(3)} = 23.3$, $^{***}p < 0.001$, Kruskal–Wallis test followed by Dunn's test, $n = 13$-16). ***I***, Distance traveled ($H_{(3)} = 23.2$, $^{***}p < 0.001$, Kruskal–Wallis test followed by Dunn's test, $n = 13$-16). ***J***, Number of entries ($H_{(3)} = 8.85$, $^{*}p = 0.031$, Kruskal–Wallis test followed by Dunn's test, $n = 13$-16) in the open arms of the EPMT ($^{**}p < 0.01$ vs gfaABC1D-EGFP group; $^{\#}p < 0.05$, $^{\#\#\#}p < 0.001$ vs DNP group). Total distance traveled by rats in the (***F***) OFT ($F_{(3,30.1)} = 10.3$, $^{***}p < 0.001$, Welch's ANOVA followed by Games–Howell test, $n = 14$-18) and (***K***) EPMT ($H_{(3)} = 11.6$, $^{**}p = 0.009$, Kruskal–Wallis test followed by Dunn's test, $n = 13$-16).

activity and morphology of vlPAG astrocytes may be closely related to DNP, which is characterized by mechanical allodynia.

vlPAG astrocytes modulate DNP-related anxiety-like behaviors

To explore the effect of vlPAG astrocytes on DNP-induced anxiety-like behavior, we conducted behavioral tests, namely, the OFT and EPMT, to assess anxiety-like behavior in DNP-model rats and ascertain whether modulation of vlPAG astrocyte activity influenced this behavior. The OFT was conducted on the 28th day after modeling. Three days later, after the previously administered CNO had completely worn off, the behavior of the rats was assessed in the EPMT (Fig. 7*A*). Compared with the control virus group, the rats in the AAV-gfaABC1D-hM4D(Gi)-EGFP group spent more time and traveled a greater distance in the center of the open field ($H_{(3)} = 33.7$, $^{***}p < 0.001$, Kruskal–Wallis test followed by Dunn's test, Fig. 7*C*; $H_{(3)} = 30.9$, $^{***}p < 0.001$, Kruskal–Wallis test followed by Dunn's test, Fig. 7*D*) and in the open arms of the EPMT ($H_{(3)} = 23.3$, $^{***}p < 0.001$, Kruskal–Wallis test followed by Dunn's test, Fig. 7*H*; $H_{(3)} = 23.2$, $^{***}p < 0.001$, Kruskal–Wallis test followed by Dunn's test, Fig.

←

one-way ANOVA followed by Tukey's multiple comparisons, $n = 6$ or 7). ***I***, Maximum branch length ($F_{(3,21)} = 4.901$, $^{*}p = 0.01$, one-way ANOVA followed by Tukey's multiple comparisons, $n = 6$ or 7) of vlPAG astrocytes expressing gfaABC1D-hM4D(Gi)-EGFP or gfaABC1D-EGFP after intraperitoneal injection of CNO ($^{**}p < 0.01$, $^{***}p < 0.001$ vs gfaABC1D-EGFP group; $^{\#}p < 0.05$, $^{\#\#\#}p < 0.001$ vs DNP group).

7*I*). Additionally, inhibition of vlPAG astrocytes increased the number of times rats entered the center of the open field ($H_{(3)}$ = 23.7, ***$p < 0.001$, Kruskal–Wallis test followed by Dunn's test, Fig. 7*E*). In contrast, no significant difference was found in entries into the open arms in the EPMT ($H_{(3)}$ = 8.85, *$p = 0.031$, Kruskal–Wallis test followed by Dunn's test, Fig. 7*J*) or in the total distance traveled in the OFT or EPMT between the virus intervention group and the control virus group ($F_{(3,30.1)}$ = 10.3, ***$p < 0.001$, Welch's ANOVA followed by Games–Howell test, Fig. 7*F*; $H_{(3)}$ = 11.6, **$p = 0.009$, Kruskal–Wallis test followed by Dunn's test, Fig. 7*K*). These results demonstrate that vlPAG astrocytes are related to DNP-induced anxiety-like behavior and that inhibition of vlPAG astrocytes reversed this phenomenon.

Activation of Gi-DREADDs in vlPAG astrocytes promotes pain-related preference in DNP-model rats

To determine whether DNP induces pain-related aversion and whether inhibition of vlPAG astrocytes using hM4D(Gi) leads to reward, we slightly modified the CPA design to create a CPP paradigm. Four weeks after modeling and virus injection, CNO treatment was paired with the white compartment (because rodents are typically photophobic) (Fig. 8*A*). After two rounds of conditioning, the rats were allowed to freely move between the two compartments. While most rats in the control virus group tended toward the black compartment ($t_{(9)}$ = 2.23, $p = 0.052$, paired *t* test, Fig. 8*B*,*C*), rats transfected with AAV-gfaABC1D-hM4D(Gi)-EGFP showed a preference for the white compartment ($t_{(9)}$ = 4.33, **$p = 0.002$, paired *t* test, Fig. 8*B*,*C*; $t_{(17.6)}$ = −3.41, **$p = 0.003$, unpaired *t* test, Fig. 8*D*). This result suggests that activation of Gi-DREADDs in vlPAG astrocytes might relieve DNP and DNP-related anxiety and motivate DNP subjects to seek the context associated with this comparative comfort (Fig. 9).

Discussion

The mechanisms underlying pain caused by peripheral neuropathy in diabetic patients are unclear and require further investigation. To this end, we first duplicated the T1DM-induced DNP model that we previously reported (J. Lu et al., 2021). The STZ-induced DNP model has been widely used in pain research (Hulse et al., 2015; Q. Huang et al., 2016; de Macedo et al., 2019; Z. Zhang et al., 2019). The Position Statement from the American Diabetes Association recommended that patients with T1DM and T2DM should be assessed annually (Pop-Busui et al., 2017). Therefore, we believe that the occurrence of DNP is a clinical endpoint of all diabetic patients. Since we focused on DNP, we adopted the T1DM-induced DNP model. As expected, typical symptoms of T1DM and DNP were induced. Moreover, we observed thermal hypoalgesia in the late stage of the model, which is consistent with previous reports (Roy Chowdhury et al., 2012; Calcutt et al., 2017).

The vlPAG is generally known to play a role in pain conduction. Many studies focusing on neurons have reported a definite link between the mPFC and vlPAG and have established a causal relationship between the existing connection and functional regulation (J. Huang et al., 2019; S. Huang et al., 2020; Drake et al., 2021). Some radiography studies have also corroborated these conclusions. A study showed that vlPAG connectivity with the higher region of the brain was strengthened in individuals with chronic pain (Mills et al., 2018), while another study located the nidus of DPN-triggered pain in the vlPAG-mediated descending pain modulation pathway using fMRI data (Segerdahl et al., 2018). Whether this enhanced connectivity in chronic pain is only mediated by neurons or regulated by other types of cells remains unclear.

Abundant evidence has established a close link between spinal astrocytes and NP (Moon et al., 2015; X. Liu et al., 2016; Z. Chen et al., 2019; Cheng et al., 2020). Chemogenetic stimulation of a unique subtype of astrocytes in spinal induced mechanical hypersensitivity (Kohro et al., 2020). Additionally, an optogenetic approach was used to activate astrocytes in the spinal dorsal horn and triggered pain hypersensitivity (Nam et al., 2016). Recent evidence suggests that astrocyte activity in the midbrain PAG is diverse in physical and inflammatory nerve injury models (Eidson and Murphy, 2013; Ni et al., 2016; Dubový et al., 2018). Direct and robust evidence that supports the role of vlPAG astrocyte function in DNP is still lacking, although some foundational work has been developed (X. Liu et al., 2022). We systematically explored differences in the temporal and spatial dimensions of PAG astrocytes and found that the activity of vlPAG astrocytes was roughly synchronized with mechanical allodynia levels, while that of other PAG subregions showed no differentiation. Interestingly, mechanical hypersensitivity was induced 7 d after modeling, yet astrocytes on day 7 were not significantly activated. We speculate that this asynchrony is because of the earlier activation of microglia than astrocytes because the transition from acute to chronic pain is because of the division of labor between these cell types (Y. J. Gao et al., 2010; Ji et al., 2013, 2019).

Gq- and Gi-DREADDs were exploited to manipulate the activity of vlPAG astrocytes. Recent evidence shows that both Gq- and Gi-signaling increases the intracellular calcium in astrocytes (Adamsky et al., 2018; Durkee et al., 2019). Interestingly, our data reveal that Gi-DREADDs cause inhibition of astrocytes. G-protein inwardly rectifying potassium channels (GIRKs) induced K^+ flux overrides Ca^{2+} flux and causes hyperpolarization may be the mechanism (Roth, 2016; Kano et al., 2019). Furthermore, calcium depletion caused by endoplasmic reticulum stress secondary to diabetes is also one of the possible mechanisms leading to the imbalance of ion levels in astrocytes (Carreras-Sureda et al., 2018).

A recent radiology study showed that metamorphoses of the nerve fascicle microstructure contribute to DPN development and pain symptoms (Jende et al., 2020). Based on these findings, we wondered whether the morphologic changes in astrocytes might also be reflected in pain symptoms. Sholl analysis is a method of assessing morphometry directly from bitmap images and has been used to analyze the morphology of neurons (Ferreira et al., 2014; Stogsdill et al., 2017). In recent years, some studies have used Sholl analysis to dissect astrocytes and microglia (T. Chen et al., 2020; MacDonald et al., 2020). Our data suggest that the morphology of vlPAG astrocytes in DNP-model rats became significantly more complex. Similarly, astrocyte processes exhibited extensive growth, and the structure became more complex during activation of Gq-DREADDs. In contrast, retardation of the growth of processes was observed when astrocytic activity was suppressed. Notably, chemogenetically manipulated astrocytes slightly differ from those in normal physiology and pathology. For example, astrocytes activated by hM3D(Gq) do not tend to increase in body volume, while astrocytes inhibited by hM4D(Gi) may not exhibit shortened maximum branch length. These data depict the association between vlPAG astrocyte architecture and DNP phenotype.

Several studies have demonstrated that the PAG, especially vlPAG neurons and neurotransmitters, governs anxiety behavior

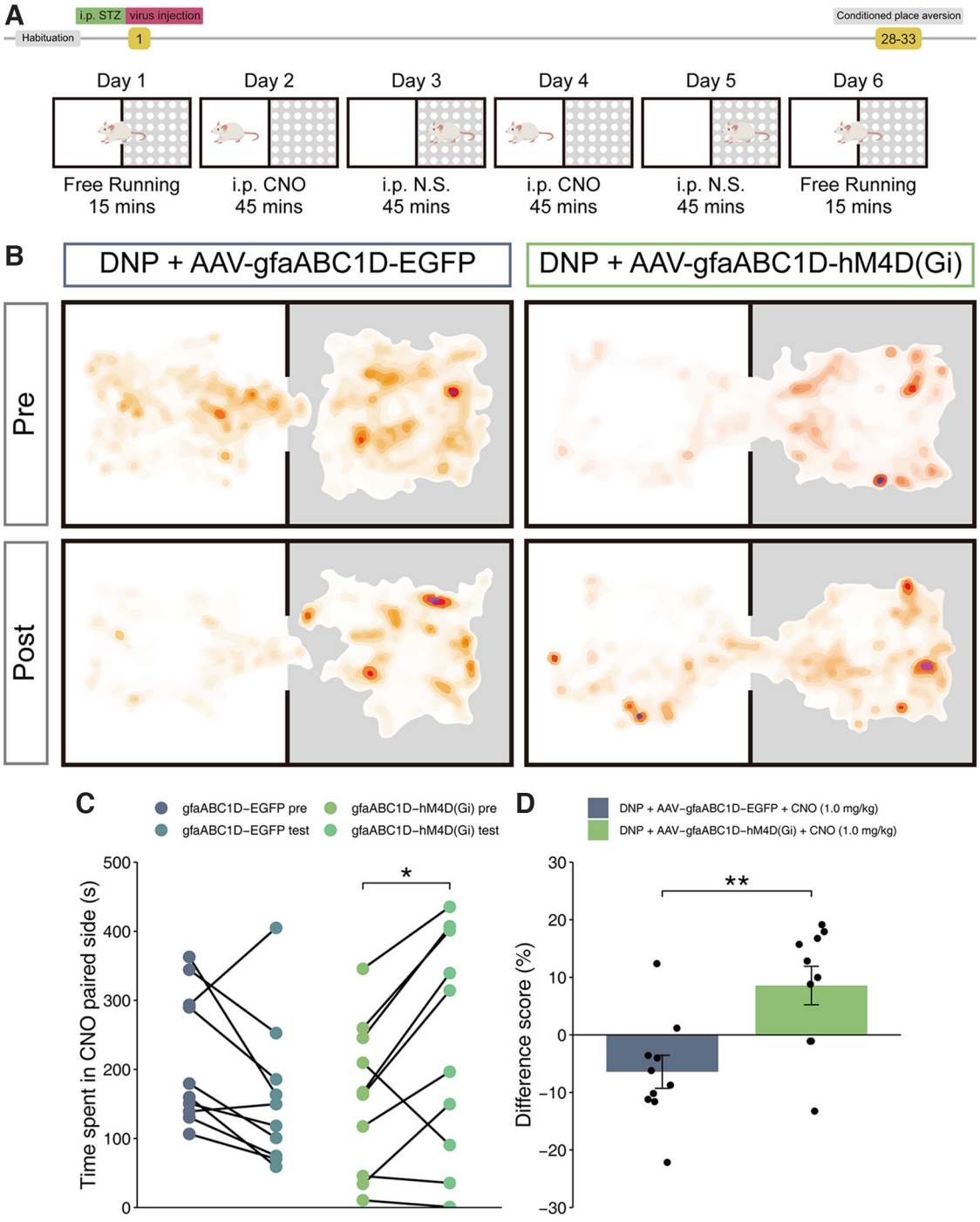

Figure 8. Gi-DREADDs selectively inhibit vlPAG astrocytes and promote CPP in DNP rats. ***A***, Schematic diagram of CPP paradigm for DNP-model rats. ***B***, Representative heatmap tracking the movements of DNP-model rats expressing gfaABC1D-hM4D(Gi)-EGFP or gfaABC1D-EGFP after treatment with CNO and conditioning to the white chamber. ***C***, Time spent in CNO-paired side (gfaABC1D-hM4D(Gi)-EGFP pretest vs test, $t_{(9)} = 4.33$, $^{**}p = 0.002$, paired *t* test, $n = 10$; gfaABC1D-EGFP pretest vs test, $t_{(9)} = 2.23$, $p = 0.052$, paired *t* test, $n = 10$). ***D***, The difference score of CPP paradigm ($t_{(17.6)} = -3.41$, $^{**}p = 0.003$, unpaired *t* test, $n = 10$).

(Nunes-de-Souza et al., 2008; Vázquez-León et al., 2018; Taylor et al., 2019). Similar changes have been found at the transcriptome level in the PAG in animal models of both NP and depression (Descalzi et al., 2017). Optogenetic activation of the dmPFC–vlPAG pathway attenuated mechanical allodynia and anxiety-like behaviors (J. B. Yin et al., 2020). In addition, an innervated microcircuit in the vlPAG regulates pain sensation and pain-related depression (W. Yin et al., 2020). Therefore, from the molecular level to that of the neural circuit, these findings support the essential role of the vlPAG in the regulation of pain-related anxiety and depression. Recent evidence has also shown that diabetes can induce depressive-like symptoms (Lenart et al., 2019). Thus, we questioned whether vlPAG astrocytes have the same regulatory ability as neurons in DNP-related anxiety behavior. Our data indicate that activation of Gi-DREADDs in vlPAG astrocytes affects the behavior of experimental animals in the OFT and EPMT. As anxiety-like behavior may be secondary to the experience of pain and may take longer to induce, we did not further investigate the behavior after astrocytes were activated by DREADDs.

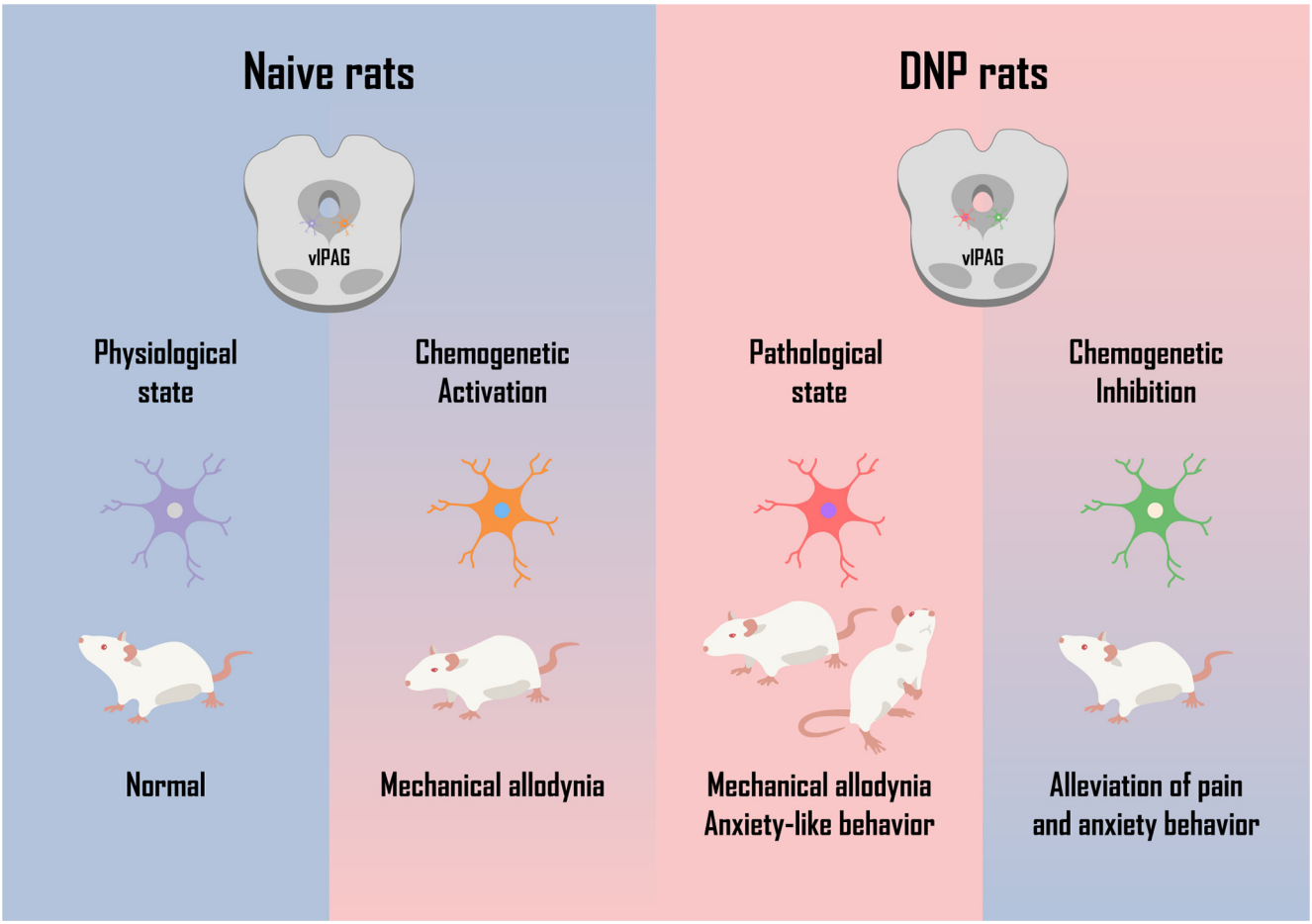

Figure 9. Graphical abstract of the study.

The CPP or CPA paradigms originating from Pavlovian conditioning are typically used to evaluate reward motivation and aversion (Cunningham et al., 2006). The PAG is an essential nucleus for coordinating fear, avoidance, and nociception behaviors (Tovote et al., 2016; Chou et al., 2018; Rozeske et al., 2018; Frontera et al., 2020). Multiple studies have used CPP or CPA to evaluate pain-related aversion (Z. Zhang et al., 2015; Llorca-Torralba et al., 2019; S. Huang et al., 2020; L. Sun et al., 2020; Wang et al., 2020). The generation of a pain-related place preference or aversion is based on a hypothetical premise, namely, that pain (similar to itchiness) (Z. R. Gao et al., 2019; Samineni et al., 2019) is a subjectively adverse physiological and emotional experience and that the individual suffering pain will pursue alleviation of this feeling (Z. Zhang et al., 2015). The principle of this hypothesis may be pain prediction error; when the actual feeling of pain exceeds the predicted value, motivated aversive learning occurs (Chou et al., 2018; George et al., 2019). The intensity of learning motivation is proportional to the amplitude of the prediction error encoded by the PAG (Roy et al., 2014). In this study, the CPA paradigm established the association between place aversion and pain. However, our observation that vlPAG astrocytes can modulate both DNP and DNP-related anxiety-like behaviors challenges the interpretation of the relationship of preference behaviors to pain or anxiety. This discrepancy may be related to the complex and extensive interactions of astrocytes with different types of neurons. Most individuals with chronic pain experience secondary, comorbid anxiety or depression (Cohen et al., 2021). Therefore, we speculate that pain relief is a major factor influencing preference behaviors in the CPP paradigm. However, we cannot rule out the possibility of DNP-related anxiety.

The neuromodulatory effects of astrocytes likely depend on astrocyte–neuron interactions, and specific molecules or proteins and their receptors may play important roles in this process. Cytokines and chemokines with their matching receptors, such as IL17-IL17R, CXCL1-CXCR2, and CXCL13-CXCR5, mediate glia–neuron interactions and regulate NP (Z. J. Zhang et al., 2013; Cao et al., 2014; Jiang et al., 2016; Luo et al., 2019). A previous study showed that, on vlPAG astrocytes, CXCL1 induced bone cancer pain through CXCR2 (Ni et al., 2019a). In addition to cytokines and chemokines, astrocytes regulate the concentration of neurotransmitters in the synaptic cleft. Studies have shown that nerve injury can lead to downregulation of the expression of the glutamate transporter 1 (GLT-1) and that overexpression of GLT-1 can reverse pain-related behavior (Falnikar et al., 2016). Our future research will focus on the interaction between vlPAG astrocytes and neurons and its association with DNP.

In conclusion, our study systematically clarified the crucial role of vlPAG astrocytes in the occurrence and development of DNP using chemogenetic interventions along with ethological and morphologic analysis. The present data consolidate current understanding of this topic, and this study is the first to report that anxiety-like behavior and DNP-related aversive motivation are regulated by vlPAG astrocytes. These findings provide new insights into DNP and its complications and supply new therapeutic targets for treating DNP (Figure 9).

References

Abbott CA, Malik RA, van Ross ER, Kulkarni J, Boulton AJ (2011) Prevalence and characteristics of painful diabetic neuropathy in a large community-based diabetic population in the U.K. Diabetes Care 34:2220–2224.

Adamsky A, Kol A, Kreisel T, Doron A, Ozeri-Engelhard N, Melcer T, Refaeli R, Horn H, Regev L, Groysman M, London M, Goshen I (2018) Astrocytic activation generates de novo neuronal potentiation and memory enhancement. Cell 174:59–71.e14.

Ahlmann-Eltze C, Patil I (2021) ggsignif: R package for displaying significance brackets for 'ggplot2.'

Allen NJ, Eroglu C (2017) Cell biology of astrocyte-synapse interactions. Neuron 96:697–708.

Bayraktar OA, et al. (2020) Astrocyte layers in the mammalian cerebral cortex revealed by a single-cell in situ transcriptomic map. Nat Neurosci 23:500–509.

Calcutt NA, Smith DR, Frizzi K, Sabbir MG, Chowdhury SK, Mixcoatl-Zecuatl T, Saleh A, Muttalib N, Van der Ploeg R, Ochoa J, Gopaul A, Tessler L, Wess J, Jolivalt CG, Fernyhough P (2017) Selective antagonism of muscarinic receptors is neuroprotective in peripheral neuropathy. J Clin Invest 127:608–622.

Cao DL, Zhang ZJ, Xie RG, Jiang BC, Ji RR, Gao YJ (2014) Chemokine CXCL1 enhances inflammatory pain and increases NMDA receptor activity and COX-2 expression in spinal cord neurons via activation of CXCR2. Exp Neurol 261:328–336.

Carreras-Sureda A, Pihán P, Hetz C (2018) Calcium signaling at the endoplasmic reticulum: fine-tuning stress responses. Cell Calcium 70:24–31.

Chen T, Lennon VA, Liu YU, Bosco DB, Li Y, Yi MH, Zhu J, Wei S, Wu LJ (2020) Astrocyte-microglia interaction drives evolving neuromyelitis optica lesion. J Clin Invest 130:4025–4038.

Chen Z, Doyle TM, Luongo L, Largent-Milnes TM, Giancotti LA, Kolar G, Squillace S, Boccella S, Walker JK, Pendleton A, Spiegel S, Neumann WL, Vanderah TW, Salvemini D (2019) Sphingosine-1-phosphate receptor 1 activation in astrocytes contributes to neuropathic pain. Proc Natl Acad Sci USA 116:10557–10562.

Cheng H, Zhang L, Xia F, Jin L, Liu S, Ren H, Zhu C, Ji Q, Tang J (2020) Astrocytic NDRG2 is critical in the maintenance of neuropathic pain. Brain Behav Immun 89:300–313.

Cheriyan J, Sheets PL (2018) Altered excitability and local connectivity of mPFC-PAG neurons in a mouse model of neuropathic pain. J Neurosci 38:4829–4839.

Chou X, Wang X, Zhang Z, Shen L, Zingg B, Huang J, Zhong W, Mesik L, Zhang LI, Tao HW (2018) Inhibitory gain modulation of defense behaviors by zona incerta. Nat Commun 9:12.

Cohen SP, Vase L, Hooten WM (2021) Chronic pain: an update on burden, best practices, and new advances. Lancet 397:2082–2097.

Colloca L, Ludman T, Bouhassira D, Baron R, Dickenson AH, Yarnitsky D, Freeman R, Truini A, Attal N, Finnerup NB, Eccleston C, Kalso E, Bennett DL, Dworkin RH, Raja SN (2017) Neuropathic pain. Nat Rev Dis Primers 3:17002.

Cunningham CL, Gremel CM, Groblewski PA (2006) Drug-induced conditioned place preference and aversion in mice. Nat Protoc 1:1662–1670.

de Macedo FH, Aires RD, Fonseca EG, Ferreira RC, Machado DP, Chen L, Zhang FX, Souza IA, Lemos VS, Romero TR, Moutal A, Khanna R, Zamponi GW, Cruz JS (2019) TNF-α mediated upregulation of NaV1.7 currents in rat dorsal root ganglion neurons is independent of CRMP2 SUMOylation. Mol Brain 12:117.

Descalzi G, Mitsi V, Purushothaman I, Gaspari S, Avrampou K, Loh YH, Shen L, Zachariou V (2017) Neuropathic pain promotes adaptive changes in gene expression in brain networks involved in stress and depression. Sci Signal 10:eaaj1549.

Drake RA, Steel KA, Apps R, Lumb BM, Pickering AE (2021) Loss of cortical control over the descending pain modulatory system determines the development of the neuropathic pain state in rats. Elife 10:e65156.

Dubový P, Klusáková I, Hradilová-Svízõenská I, Joukal M, Boadas-Vaello P (2018) Activation of astrocytes and microglial cells and CCL2/CCR2 upregulation in the dorsolateral and ventrolateral nuclei of periaqueductal gray and rostral ventromedial medulla following different types of sciatic nerve injury. Front Cell Neurosci 12:40.

Durkee CA, Covelo A, Lines J, Kofuji P, Aguilar J, Araque A (2019) $G_{i/o}$ protein-coupled receptors inhibit neurons but activate astrocytes and stimulate gliotransmission. Glia 67:1076–1093.

Dyck PJ, Albers JW, Andersen H, Arezzo JC, Biessels GJ, Bril V, Feldman EL, Litchy WJ, O'Brien PC, Russell JW, Toronto Expert Panel on Diabetic Neuropathy (2011) Diabetic polyneuropathies: update on research definition, diagnostic criteria and estimation of severity: diabetic polyneuropathies. Diabetes Metab Res Rev 27:620–628.

Eidson LN, Murphy AZ (2013) Persistent peripheral inflammation attenuates morphine-induced periaqueductal gray glial cell activation and analgesic tolerance in the male rat. J Pain 14:393–404.

Falnikar A, Hala TJ, Poulsen DJ, Lepore AC (2016) GLT1 overexpression reverses established neuropathic pain-related behavior and attenuates chronic dorsal horn neuron activation following cervical spinal cord injury: GLT1 overexpression reverses neuropathic pain-related behavior. Glia 64:396–406.

Feldman EL, Callaghan BC, Pop-Busui R, Zochodne DW, Wright DE, Bennett DL, Bril V, Russell JW, Viswanathan V (2019) Diabetic neuropathy. Nat Rev Dis Primers 5:41.

Ferreira TA, Blackman AV, Oyrer J, Jayabal S, Chung AJ, Watt AJ, Sjöström PJ, van Meyel DJ (2014) Neuronal morphometry directly from bitmap images. Nat Methods 11:982–984.

Finnerup NB, Kuner R, Jensen TS (2021) Neuropathic pain: from mechanisms to treatment. Physiol Rev 101:259–301.

Frontera JL, Baba Aissa H, Sala RW, Mailhes-Hamon C, Georgescu IA, Léna C, Popa D (2020) Bidirectional control of fear memories by cerebellar neurons projecting to the ventrolateral periaqueductal grey. Nat Commun 11:5207.

Gao YJ, Xu ZZ, Liu YC, Wen YR, Decosterd I, Ji RR (2010) The c-Jun N-terminal kinase 1 (JNK1) in spinal astrocytes is required for the maintenance of bilateral mechanical allodynia under a persistent inflammatory pain condition. Pain 148:309–319.

Gao ZR, Chen WZ, Liu MZ, Chen XJ, Wan L, Zhang XY, Yuan L, Lin JK, Wang M, Zhou L, Xu XH, Sun YG (2019) Tac1-expressing neurons in the periaqueductal gray facilitate the itch-scratching cycle via descending regulation. Neuron 101:45–59.e9.

George DT, Ameli R, Koob GF (2019) Periaqueductal gray sheds light on dark areas of psychopathology. Trends Neurosci 42:349–360.

Hargreaves K, Dubner R, Brown F, Flores C, Joris J (1988) A new and sensitive method for measuring thermal nociception in cutaneous hyperalgesia. Pain 32:77–88.

Herculano-Houzel S (2014) The glia/neuron ratio: how it varies uniformly across brain structures and species and what that means for brain physiology and evolution: the glia/neuron ratio. Glia 62:1377–1391.

Huang J, Gadotti VM, Chen L, Souza IA, Huang S, Wang D, Ramakrishnan C, Deisseroth K, Zhang Z, Zamponi GW (2019) A neuronal circuit for activating descending modulation of neuropathic pain. Nat Neurosci 22:1659–1668.

Huang Q, Chen Y, Gong N, Wang YX (2016) Methylglyoxal mediates streptozotocin-induced diabetic neuropathic pain via activation of the peripheral TRPA1 and Nav1.8 channels. Metabolism 65:463–474.

Huang S, Zhang Z, Gambeta E, Xu SC, Thomas C, Godfrey N, Chen L, M'Dahoma S, Borgland SL, Zamponi GW (2020) Dopamine inputs from the ventral tegmental area into the medial prefrontal cortex modulate neuropathic pain-associated behaviors in mice. Cell Rep 31:107812.

Hulse RP, Beazley-Long N, Ved N, Bestall SM, Riaz H, Singhal P, Ballmer Hofer K, Harper SJ, Bates DO, Donaldson LF (2015) Vascular endothelial growth factor-A165b prevents diabetic neuropathic pain and sensory neuronal degeneration. Clin Sci (Lond) 129:741–756.

Iadecola C, Nedergaard M (2007) Glial regulation of the cerebral microvasculature. Nat Neurosci 10:1369–1376.

IASP (2022) IASP taxonomy. Available at https://www.iasp-pain.org/resources/terminology/#pain.

Jende JM, Groener JB, Kender Z, Rother C, Hahn A, Hilgenfeld T, Juerchott A, Preisner F, Heiland S, Kopf S, Nawroth P, Bendszus M, Kurz FT (2020) Structural nerve remodeling at 3-T MR neurography differs between painful and painless diabetic polyneuropathy in type 1 or 2 diabetes. Radiology 294:405–414.

Jensen TS, Finnerup NB (2014) Allodynia and hyperalgesia in neuropathic pain: clinical manifestations and mechanisms. Lancet Neurol 13:924–935.

Ji RR, Berta T, Nedergaard M (2013) Glia and pain: is chronic pain a gliopathy? Pain 154:S10–S28.

Ji RR, Donnelly CR, Nedergaard M (2019) Astrocytes in chronic pain and itch. Nat Rev Neurosci 20:667–685.

Jiang BC, Cao DL, Zhang X, Zhang ZJ, He LN, Li CH, Zhang WW, Wu XB, Berta T, Ji RR, Gao YJ (2016) CXCL13 drives spinal astrocyte activation and neuropathic pain via CXCR5. J Clin Invest 126:745–761.

Kano H, Toyama Y, Imai S, Iwahashi Y, Mase Y, Yokogawa M, Osawa M, Shimada I (2019) Structural mechanism underlying G protein family-specific regulation of G protein-gated inwardly rectifying potassium channel. Nat Commun 10:2008.

Kassambara A (2021) rstatix: pipe-friendly framework for basic statistical tests. Available at https://CRAN.R-project.org/package=rstatix.

Kohro Y, et al. (2020) Spinal astrocytes in superficial laminae gate brainstem descending control of mechanosensory hypersensitivity. Nat Neurosci 23:1376–1387.

Lenart L, Balogh DB, Lenart N, Barczi A, Hosszu A, Farkas T, Hodrea J, Szabo AJ, Szigeti K, Denes A, Fekete A (2019) Novel therapeutic potential of angiotensin receptor 1 blockade in a rat model of diabetes-associated depression parallels altered BDNF signalling. Diabetologia 62:1501–1513.

Li L, Chen J, Wang J, Cai D (2015) Prevalence and risk factors of diabetic peripheral neuropathy in Type 2 diabetes mellitus patients with overweight/obese in Guangdong province, China. Prim Care Diabetes 9:191–195.

Liu F, Bao Y, Hu R, Zhang X, Li H, Zhu D, Li Y, Yan L, Li Y, Lu J, Li Q, Zhao Z, Ji Q, Jia W (2010) Screening and prevalence of peripheral neuropathy in type 2 diabetic outpatients: a randomized multicentre survey in 12 city hospitals of China. Diabetes Metab Res Rev 26:481–489.

Liu X, Liu H, Xu S, Tang Z, Xia W, Cheng Z, Li W, Jin Y (2016) Spinal translocator protein alleviates chronic neuropathic pain behavior and modulates spinal astrocyte–neuronal function in rats with L5 spinal nerve ligation model. Pain 157:103–116.

Liu X, He J, Gao J, Xiao Z (2022) Fluorocitrate and neurotropin confer analgesic effects on neuropathic pain in diabetic rats via inhibition of astrocyte activation in the periaqueductal gray. Neurosci Lett 768:136378.

Llorca-Torralba M, Suárez-Pereira I, Bravo L, Camarena-Delgado C, Garcia-Partida JA, Mico JA, Berrocoso E (2019) Chemogenetic silencing of the locus coeruleus–basolateral amygdala pathway abolishes pain-induced anxiety and enhanced aversive learning in rats. Biol Psychiatry 85:1021–1035.

Lu J, Yang L, Xu Y, Ai L, Chen J, Xiong F, Hu L, Chen H, Liu J, Yan X, Huang H, Chen L, Yu C (2021) The modulatory effect of motor cortex astrocytes on diabetic neuropathic pain. J Neurosci 41:5287–5302.

Lu Y, Xing P, Cai X, Luo D, Li R, Lloyd C, Sartorius N, Li M (2020) Prevalence and risk factors for diabetic peripheral neuropathy in type 2 diabetic patients from 14 countries: estimates of the INTERPRET-DD Study. Front Public Health 8:534372.

Luo H, Liu HZ, Zhang WW, Matsuda M, Lv N, Chen G, Xu ZZ, Zhang YQ (2019) Interleukin-17 regulates neuron-glial communications, synaptic transmission, and neuropathic pain after chemotherapy. Cell Rep 29:2384–2397.e5.

MacDonald AJ, Holmes FE, Beall C, Pickering AE, Ellacott KL (2020) Regulation of food intake by astrocytes in the brainstem dorsal vagal complex. Glia 68:1241–1254.

Micheli L, Rajagopalan R, Lucarini E, Toti A, Parisio C, Carrino D, Pacini A, Ghelardini C, Rajagopalan P, Di Cesare Mannelli L (2021) Pain relieving and neuroprotective effects of non-opioid compound, DDD-028, in the rat model of paclitaxel-induced neuropathy. Neurotherapeutics 18:2008–2020.

Mills EP, Di Pietro F, Alshelh Z, Peck CC, Murray GM, Vickers ER, Henderson LA (2018) Brainstem pain-control circuitry connectivity in chronic neuropathic pain. J Neurosci 38:465–473.

Mitrirattanakul S, Ramakul N, Guerrero AV, Matsuka Y, Ono T, Iwase H, Mackie K, Faull KF, Spigelman I (2006) Site-specific increases in peripheral cannabinoid receptors and their endogenous ligands in a model of neuropathic pain. Pain 126:102–114.

Moon JY, Choi SR, Roh DH, Yoon SY, Kwon SG, Choi HS, Kang SY, Han HJ, Kim HW, Beitz AJ, Oh SB, Lee JH (2015) Spinal sigma-1 receptor activation increases the production of D-serine in astrocytes which contributes to the development of mechanical allodynia in a mouse model of neuropathic pain. Pharmacol Res 100:353–364.

Morgan MM, Whittier KL, Hegarty DM, Aicher SA (2008) Periaqueductal gray neurons project to spinally projecting GABAergic neurons in the rostral ventromedial medulla. Pain 140:376–386.

Nam Y, Kim JH, Kim JH, Jha MK, Jung JY, Lee MG, Choi IS, Jang IS, Lim DG, Hwang SH, Cho HJ, Suk K (2016) Reversible induction of pain hypersensitivity following optogenetic stimulation of spinal astrocytes. Cell Rep 17:3049–3061.

National Research Council (2010) Guide for the care and use of laboratory animals. Washington, DC: National Research Council.

Ni H, Yao M, Huang B, Xu LS, Zheng Y, Chu YX, Wang HQ, Liu MJ, Xu SJ, Li HB (2016) Glial activation in the periaqueductal gray promotes descending facilitation of neuropathic pain through the p38 MAPK signaling pathway: glial activation, neuropathic pain, and the p38 MAPK signaling pathway. J Neurosci Res 94:50–61.

Ni H, Wang Y, An K, Liu Q, Xu L, Zhu C, Deng H, He Q, Wang T, Xu M, Zheng Y, Huang B, Fang J, Yao M (2019a) Crosstalk between NFκB-dependent astrocytic CXCL1 and neuron CXCR2 plays a role in descending pain facilitation. J Neuroinflammation 16:1.

Ni H, Xu LS, Wang Y, Li H, An K, Liu M, Liu Q, Deng H, He Q, Huang B, Fang J, Yao M (2019b) Astrocyte activation in the periaqueductal gray promotes descending facilitation to cancer-induced bone pain through the JNK MAPK signaling pathway. Mol Pain 15:1744806919831909.

Nunes-de-Souza V, Nunes-de-Souza RL, Rodgers RJ, Canto-de-Souza A (2008) 5-HT2 receptor activation in the midbrain periaqueductal grey (PAG) reduces anxiety-like behaviour in mice. Behav Brain Res 187:72–79.

Pan Q, Li Q, Deng W, Zhao D, Qi L, Huang W, Ma L, Li H, Li Y, Lyu X, Wang A, Yao H, Xing X, Guo L (2018) Prevalence of and risk factors for peripheral neuropathy in Chinese patients with diabetes: a multicenter cross-sectional study. Front Endocrinol 9:617.

Pop-Busui R, Boulton AJ, Feldman EL, Bril V, Freeman R, Malik RA, Sosenko JM, Ziegler D (2017) Diabetic neuropathy: a position statement by the American Diabetes Association. Diabetes Care 40:136–154.

R Core Team (2021) R: a language and environment for statistical computing. Available at https://www.R-project.org/.

Roth BL (2016) DREADDs for neuroscientists. Neuron 89:683–694.

Roy Chowdhury SK, Smith DR, Saleh A, Schapansky J, Marquez A, Gomes S, Akude E, Morrow D, Calcutt NA, Fernyhough P (2012) Impaired adenosine monophosphate-activated protein kinase signalling in dorsal root ganglia neurons is linked to mitochondrial dysfunction and peripheral neuropathy in diabetes. Brain 135:1751–1766.

Roy M, Shohamy D, Daw N, Jepma M, Wimmer GE, Wager TD (2014) Representation of aversive prediction errors in the human periaqueductal gray. Nat Neurosci 17:1607–1612.

Rozeske RR, Jercog D, Karalis N, Chaudun F, Khoder S, Girard D, Winke N, Herry C (2018) Prefrontal-periaqueductal gray-projecting neurons mediate context fear discrimination. Neuron 97:898–910.e6.

RStudio Team (2020) RStudio: integrated development environment for R. Available at http://www.rstudio.com/.

Samineni VK, Premkumar LS, Faingold CL (2017) Neuropathic pain-induced enhancement of spontaneous and pain-evoked neuronal activity in the periaqueductal gray that is attenuated by gabapentin. Pain 158:1241–1253.

Samineni VK, Grajales-Reyes JG, Sundaram SS, Yoo JJ, Gereau RW (2019) Cell type-specific modulation of sensory and affective components of itch in the periaqueductal gray. Nat Commun 10:4356.

Schindelin J, Arganda-Carreras I, Frise E, Kaynig V, Longair M, Pietzsch T, Preibisch S, Rueden C, Saalfeld S, Schmid B, Tinevez JY, White DJ, Hartenstein V, Eliceiri K, Tomancak P, Cardona A (2012) Fiji: an open-source platform for biological-image analysis. Nat Methods 9:676–682.

Segerdahl AR, Themistocleous AC, Fido D, Bennett DL, Tracey I (2018) A brain-based pain facilitation mechanism contributes to painful diabetic polyneuropathy. Brain 141:357–364.

Selvarajah D, Kar D, Khunti K, Davies MJ, Scott AR, Walker J, Tesfaye S (2019) Diabetic peripheral neuropathy: advances in diagnosis and strategies for screening and early intervention. Lancet Diabetes Endocrinol 7:938–948.

Stogsdill JA, Ramirez J, Liu D, Kim YH, Baldwin KT, Enustun E, Ejikeme T, Ji RR, Eroglu C (2017) Astrocytic neuroligins control astrocyte morphogenesis and synaptogenesis. Nature 551:192–197.

Sun J, Wang Y, Zhang X, Zhu S, He H (2020) Prevalence of peripheral neuropathy in patients with diabetes: a systematic review and meta-analysis. Prim Care Diabetes 14:435–444.

Sun L, Liu R, Guo F, Wen MQ, Ma XL, Li KY, Sun H, Xu CL, Li YY, Wu MY, Zhu ZG, Li XJ, Yu YQ, Chen Z, Li XY, Duan S (2020) Parabrachial nucleus circuit governs neuropathic pain-like behavior. Nat Commun 11:5974.

Sun Y, Wang J, Liang SH, Ge J, Lu YC, Li JN, Chen YB, Luo DS, Li H, Li YQ (2020) Involvement of the ventrolateral periaqueductal gray matter-central medial thalamic nucleus-basolateral amygdala pathway in neuropathic pain regulation of rats. Front Neuroanat 14:32.

Taylor NE, Pei J, Zhang J, Vlasov KY, Davis T, Taylor E, Weng FJ, Van Dort CJ, Solt K, Brown EN (2019) The role of glutamatergic and dopaminergic neurons in the periaqueductal gray/dorsal raphe: separating analgesia and anxiety. eNeuro 6:ENEURO.0018-18.2019.

Tesfaye S, Boulton AJ, Dickenson AH (2013) Mechanisms and management of diabetic painful distal symmetrical polyneuropathy. Diabetes Care 36:2456–2465.

Tovote P, Esposito MS, Botta P, Chaudun F, Fadok JP, Markovic M, Wolff SB, Ramakrishnan C, Fenno L, Deisseroth K, Herry C, Arber S, Lüthi A (2016) Midbrain circuits for defensive behaviour. Nature 534:206–212.

Vázquez-León P, Campos-Rodríguez C, Gonzalez-Pliego C, Miranda-Páez A (2018) Differential effects of cholecystokinin (CCK-8) microinjection into the ventrolateral and dorsolateral periaqueductal gray on anxiety models in Wistar rats. Horm Behav 106:105–111.

Wang H, Dong P, He C, Feng XY, Huang Y, Yang WW, Gao HJ, Shen XF, Lin S, Cao SX, Lian H, Chen J, Yan M, Li XM (2020) Incerta-thalamic circuit controls nocifensive behavior via cannabinoid type 1 receptors. Neuron 107:538–551.e5.

Wickham H (2016) ggplot2: elegant graphics for data analysis. New York: Springer.

Yin JB, et al. (2020) dmPFC–vlPAG projection neurons contribute to pain threshold maintenance and antianxiety behaviors. J Clin Invest 130:6555–6570.

Yin W, Mei L, Sun T, Wang Y, Li J, Chen C, Farzinpour Z, Mao Y, Tao W, Li J, Xie W, Zhang Z (2020) A central amygdala–ventrolateral periaqueductal gray matter pathway for pain in a mouse model of depression-like behavior. Anesthesiology 132:1175–1196.

Yu W, Pati D, Pina MM, Schmidt KT, Boyt KM, Hunker AC, Zweifel LS, McElligott ZA, Kash TL (2021) Periaqueductal gray/dorsal raphe dopamine neurons contribute to sex differences in pain-related behaviors. Neuron 109:1365–1380.e5.

Zhang Y, et al. (2021) Painful Diabetic Peripheral Neuropathy Study of Chinese Outpatients (PDNSCOPE): a multicentre cross-sectional registry study of clinical characteristics and treatment in Mainland China. Pain Ther 10:1355–1373.

Zhang Z, Gadotti VM, Chen L, Souza IA, Stemkowski PL, Zamponi GW (2015) Role of prelimbic GABAergic circuits in sensory and emotional aspects of neuropathic pain. Cell Rep 12:752–759.

Zhang Z, Ding X, Zhou Z, Qiu Z, Shi N, Zhou S, Du L, Zhu X, Wu Y, Yin X, Zhou C (2019) Sirtuin 1 alleviates diabetic neuropathic pain by regulating synaptic plasticity of spinal dorsal horn neurons. Pain 160:1082–1092.

Zhang ZJ, Cao DL, Zhang X, Ji RR, Gao YJ (2013) Chemokine contribution to neuropathic pain: respective induction of CXCL1 and CXCR2 in spinal cord astrocytes and neurons. Pain 154:2185–2197.

Zhou Y, Zhu H, Liu Z, Chen X, Su X, Ma C, Tian Z, Huang B, Yan E, Liu X, Ma L (2019) A ventral CA1 to nucleus accumbens core engram circuit mediates conditioned place preference for cocaine. Nat Neurosci 22:1986–1999.